Control of chimera states in oscillator networks

PhD Thesis

Giulia Ruzzene

TESI DOCTORAL UPF / 2020

DIRECTOR DE LA TESI:

Prof. Dr. Ralph G. Andrzejak

Universitat Pompeu Fabra, Department DTIC

A tutti i miei insegnanti.

To all my teachers.

Acknowledgements

Italian engineer and astrophysicist Amalia Ercoli-Finzi said in an interview in 2018 that to succeed as a woman you need three halves: iron health, steel nerves and a golden husband. Writing this PhD thesis during a global pandemic gave new meaning to the first half. The whole PhD process helped me to develop the second half and taught me the importance of having a supportive partner, without forgetting how important it is to be independent and self-sufficient. For all of this I am grateful.

I would like to thank my advisor, Prof. Dr. Ralph G. Andrzejak, for giving me the opportunity to do this PhD in Barcelona, which feels like home to me. I would like to thank him for the valuable lessons and for introducing me to scientists from all over the world, by giving me the possibility to travel to many conferences.

Of all the scientists I met during this PhD, I am especially grateful to Prof. Dr. Eckehard Schöll for inviting me to Berlin and make me feel part of his group for four months, which were the beginning of an enduring collaboration. I would like to thank Dr. Anna Zakharova for supervising my work while I was there and Dr. Iryna Omelchenko for the many fruitful discussions. I value their example as women in science. I would also like to thank Dr. Jakub Sawicki, Rico Berner and all the students of Prof. Schöll's group.

Teaching activities were an important part of my PhD and I am grateful to have been part of a great team led by Prof. Vanesa Daza Fernandez. It was a pleasure to work with all the Linear Algebra people.

A special thought for all the people of office 55.117, in random order: Petroula, Marc, Federico, Irene, Ola, Cristina, Angela, Anaïs, and also for the guests and neighbours Marco, Mario, Paola and for all the students who worked in our group.

I would like to dedicate this thesis also to my fellow Math students in Udine, because through our Aula Studio Matematici I learned the importance of being part of a (fun) community in science and I admire all of their talent.

Thank you Giulia, Mariachiara and Chiara for your friendship and long-distance support. Thank you Fernanda, our vacation in Brazil in 2016 made me arrive to Barcelona with the right spirit and I hope we can resume our meetings in different continents soon.

Grazie alla mia famiglia estesa, tutte le mie zie, zii e cugini che sono sempre pronti ad accogliermi quando torno a casa e sono sempre molto (troppo) fieri di quello che faccio.

Un grazie più grande però ai miei genitori. Per accettare che sto lontano da casa, per non farmi mancare mai nulla e per tutte le cose che mi hanno insegnato. Vi voglio bene.

Gràcies Marc per ser tu, per fer-me riure y per estar sempre al meu costat des de qualsevol lloc. T'estimo.

Abstract

Partial synchronization is an important phenomenon observed in nature and model systems. Chimera states are the most studied type of partially synchronized dynamics and attract interest from many fields of science. In homogeneous networks of identical oscillators, a chimera state is a symmetry broken dynamics in which the oscillators spontaneously split into two complementary groups: one in which they are synchronized and one in which they are not. The quest for chimera states in real-world scenarios has been made challenging by their unstable nature in systems of finite size. Therefore, it became crucial to find ways to control them. In this thesis we propose a new control method based on a pacemaker oscillator. We show how it can control all of the chimeras' instabilities in networks of phase oscillators and we generalized this concept to more complex scenarios by applying it to multiplex networks of phase and FitzHugh-Nagumo oscillators.

Keywords: Chimera states, control, synchronization, oscillator networks.

Resum

La sincronització parcial és un fenomen que s'observa en la naturalesa i en models matemàtics. Els anomenats estats quimera són entre els exemples més estudiats de sincronització parcial i atrauen l'interès de molts àmbits científics. En xarxes homogènies d'oscil·ladors idèntics, un estat quimera és una dinàmica en què es trenca la simetria perquè els oscil·ladors es divideixen espontàniament en dos grups complementaris: en un grup estan sincronitzats i en l'altre no. La cerca d'estats de quimera en escenaris del món real s'ha vist dificultada per la seva naturalesa inestable en sistemes finits. Per tant, és crucial trobar formes de controlar-les. En aquesta tesi proposem un nou mètode de control que utilitza un pacemaker (oscil·lador marcapassos). Mostrem com el pacemaker pot controlar totes les inestabilitats de les quimeres en xarxes d'oscil·ladors de fase i generalitzem aquest concepte a escenaris més complexos aplicant-lo a xarxes formades per capes d'oscil·ladors de fases i models de neurones de FitzHugh-Nagumo.

Paraules claus: estats quimera, control, sincronització, xarxes d'oscil·ladors.

Resumen

La sincronización parcial es un fenómeno importante que se observa en la naturaleza y en modelos matemáticos. Los denominados estados quimera son el tipo más estudiado de dinámica parcialmente sincronizada y atraen el interés de muchos campos de la ciencia. En redes homogéneas de osciladores idénticos, un estado quimera es una dinámica con simetría rota en la que los osciladores se dividen espontáneamente en dos grupos complementarios: en uno están sincronizados y en el otro no. La investigación de estados quimera en escenarios reales se ha convertido en un desafío por su naturaleza inestable en sistemas finitos. Por lo tanto, es crucial encontrar forma de controlarlos. En esta tesis proponemos un nuevo método de control basado en un oscilador marcapasos (pacemaker). Mostramos cómo esto puede controlar las inestabilidades de las quimeras en redes de osciladores de fase y generalizamos el concepto a escenarios más complejos al aplicarlo a redes multi-capa de osciladores de fase y de modelos de neuronas de FitzHugh-Nagumo.

Palabras claves: estados quimera, control, sincronización, redes de osciladores.

Sinossi

La sincronizzazione parziale è un fenomeno che si osserva in natura e in modelli matematici. I cosiddetti stati chimera sono uno dei piú studiati esempi di sincronizzazione parziale e hanno suscitato interesse in molti ambiti scientifici. In reti omogenee di oscillatori identici, uno stato chimera è una dinamica in cui si rompe la simmetria, poiché gli oscillatori si dividono spontaneamente in due gruppi complementari: in uno sono sincronizzati e nell'altro no. La ricerca di stati chimera nel mondo reale è resa difficile dalla loro natura instabile in sistemi finiti. Per questo motivo, è di cruciale importanza trovare modi per controllare questi stati. In questa tesi proponiamo un nuovo metodo di controllo che si basa sull'idea di un pacemaker. Dimostriamo che un pacemaker può controllare tutte le instabilità degli stati chimera in reti di oscillatori di fase. Inoltre, generalizziamo questo concetto a scenari più complessi applicandolo a reti formate da più strati di oscillatori di fase e modelli di neuroni di FitzHugh-Nagumo.

Parole chiave: stati chimera, controllo, sincronizzazione, reti di oscillatori

List of Publications

Ruzzene G., Omelchenko I., Sawicki J. and Zakharova A., Schöll E., Andrzejak R. G., *Remote pacemaker control of chimera states in multilayer neuronal networks*, in preparation (2020)

Andrzejak R. G., Ruzzene G., Schöll E., Omelchenko I., *Two populations of coupled quadratic maps exhibit a plentitude of symmetric and symmetry broken dynamics*, Chaos: an Interdisciplinary Journal of Nonlinear Science, 30, 033125 (2020)

Ruzzene G., Omelchenko I., Schöll, E., Zakharova A., Andrzejak R. G., *Control of chimera states via minimal coupling modification*, Chaos: an Interdisciplinary Journal of Nonlinear Science, 29, 051103 (2019)

Andrzejak R. G., Ruzzene G., Malvestio I., Schindler K., Schöll, E., Zakharova A., *Mean-field phase synchronization between chimera states*, Chaos: an Interdisciplinary Journal of Nonlinear Science, 28, 091101 (2018)

Andrzejak R. G., Ruzzene G., Malvestio I., *Generalized synchronization between chimera states*, Chaos: an Interdisciplinary Journal of Nonlinear Science, 27, 053114 (2017)

Contents

CHAPTER 1

Introduction

Synchronization is a fundamental and universal concept in nature, technology and human life [74]. From fireflies lighintg up in synchrony, crowds clapping in unison, neurons in the brain firing simultaneously, to power generators maintaing the same frequency in a power grid, the examples are abundant and come from all sorts of fields [15]. In 1665, the Dutch physicist Christian Huygens observed two coupled pendulum clocks synchronizing and started to investigate a phenomenon that later turned out to be omnipresent in natural and man-made systems. It was not until 1967 that synchronization was given a formal mathematical framework by Art Winfree [103]. His equations are the foundation for a variety of models that are used nowadays to simulate the behaviour of systems of coupled oscillators. The most famous model that originated from Winfree's equations is undoubtedly the Kuramoto model, proposed by Japanese physicist Yoshiki Kuramoto in 1974 [46]. Kuramoto's equations were born as an attempt to simplify Winfree's model and

they became ubiquitous in the study of globally coupled systems. Despite its wide applicability, the Kuramoto model has one limitation: it describes the transition to global synchronization, a state where all the components of the system become synchronized. But at the beginning of the new millenium it became clear that global synchronization is only part of a bigger picture.

In 2002, Kuramoto and Battogtokh discovered a new kind of partially synchronized spatiotemporal pattern emerging in a ring network of nonlocally coupled phase oscillators [47]. On a ring, oscillators are nonlocally coupled if each one of them is connected only to some of its nearest neighbours. This is an intermediate configuration between global coupling and local coupling, in which each oscillator is coupled only to its two nesarest neighbours. The authors observed that the spatial rotational symmetry is not preserved in the evolution of the dynamics. The oscillators spontaneously split into two complementary groups: one in which they are synchronized and one in which they perform a seemingly erratic motion. This peculiar phenomenon was then named chimera state by Abrams and Strogatz in 2004 [3]. After a few years, chimera states became one of the most studied partially synchronized dynamics. Research on chimera states developed in many different directions, going towards more complex models in which they can appear and unveiling analogies with various real-world phenomena.

After their discovery in ring networks of phase oscillators, chimeras were observed in networks formed by oscillators with more complex dynamics. In 2013, Omelchenko et al. observed chimera states in networks of FitzHugh-Nagumo oscillatory units, which model features of neuronal dynamics [69]. In the following year, Hizanidis and coauthors observed chimera states in networks of nonlocally coupled Hindmarsch-Rose neuron models [36]. Chimera states also appear in networks of Stuart-Landau oscillators [90]. Here they take the form of amplitude chimeras, which were

also later reported in Ref. [108]. In Ref. [65], the authors reported the appearence of chimera states in networks of van der Pol oscillators. Furthermore, chimera patterns also appear in networks of time discrete maps, as it was shown for the first time by Omelchenko and colleagues in Ref. [64]. Subsequently chimeras have been found in networks and ensembles of logistic maps [8, 17–19, 28, 67, 101], Hénon maps [20, 85, 92, 93] and other types of time-discrete maps [8, 35, 62, 95].

Not only have chimeras been observed for different types of oscillators and maps, but also in networks with topologies that are far more complex than the ring structure originally considered by Kuramoto in 2002. For example, the previously mentioned study with Stuart-Landau oscillators used a spatially extended system with global coupling [90]. Spatial configurations with two and three dimensions have also been used as models to generate chimera states [41, 53, 71, 84]. Interestingly, they can also emerge in bidimensional networks with fractal topologies [22, 76, 88]. Also, increasing the complexity of the interactions between the network nodes can lead to the formation of chimera states in more sophisticated scenarios. For example the introduction of delays has an impact on the emergence of chimera states [14, 94, 107]. Furthermore, chimeras can appear in phase oscillator networks in which the coupling function includes higher order harmonics [14, 98]. Another important category of structures in which chimera states have been observed is the one formed by populations of oscillators. In this case the oscillators are coupled all to all within a population and weakly across populations. This type of structure was considered by Montbrió and coauthors in Ref. [60], where they studied how oscillators synchronize in interacting populations, and found chimera patterns. Other examples of chimera states in populations of oscillators were studied also from an analytical point of view in Refs. [2, 48].

Given that real systems are rarely isolated but instead are almost always interacting among them, scientists also explored the possibility of obtaining chimera states in multilayer networks. This line of research developed only recently and opened a path to obtaining richer dynamical profiles and synchronization scenarios. In multilayer networks the interactions among the nodes are classified into different groups which correspond to different layers and there are also interactions among the layers [4, 16, 42]. For example, transportation networks can be modelled as multilayer networks, since different places may be connected by different means of transport [24]. The brain can be seen as a multilayer network, as one might picture a layer corresponding to the anatomical network and one to the functional network [12]. Many other examples show how powerful multilayer modelling is and how important it is to extend previous theoretical studies in single-layer networks to this new, richer scenario. The research on chimera states in multilayer networks has focused mainly on a subcategory of these networks known as multiplex networks. In the literature about chimera states, multiplex networks are structures in which all the layers have the same type and number of nodes and the coupling is one-to-one among nodes belonging to different layers. Furthermore, in this configuration one can introduce mismatches in the parameters of oscillators belonging to different layers. In classical network science papers, in multiplex networks all layers are supposed to be identical [4, 16, 42]. Chimera states were observed in two- and three-layer multiplex networks of Hindmarsh-Rose neurons in Ref. [57]. In Refs. [54, 55], Majhi and coauthors considered a two-layer network of Hindmarsh-Rose neurons and observed the emergence of chimera states via multiplexing when the neurons were uncoupled in one of the two layers. When there are different interacting layers, it is important to study if and how their dynamics synchronize. In the study in Ref. [5] the authors detected generalized

synchronization between chimera states in a two-layer network of phase oscillators. In [87] it was shown that in a multiplex scheme with three layers formed by ring networks of FitzHugh-Nagumo oscillators, time delays can control relay synchronization between chimera states. For a two-layer network of oscillatory FitzHugh-Nagumo units, a control strategy based on weak multiplexing was developed allowing to induce or suppress chimera states [59]. As we said, all the previous studies are focused on multiplex networks. In Ref. [7] for the first time, the authors observed chimera states in a network with layers of different sizes. They modelled a mean field interlayer coupling and observed that the phases of the order parameters of the two layers synchronize forming Arnold-tongues in the parameter space [7].

This rich body of research on chimera states based on analytical results and numerical simulations in the context of coupled oscillators was accompanied by the discovery of analogies between chimera states and real-world phenomena. Since synchronization in general is so fundamental in many natural and technological processes, it is only natural to ask if such peculiar partial synchronization phenomena such as chimera states can be observed in real-world systems or engineered in the lab. The connections between partial synchronization and neuroscience opened a fascinating research line in the past decade. In their seminal 2004 paper [3], Abrams and Strogatz already suggested an analogy between chimera states and unihemispheric sleep in dolphins and birds [79]. This analogy was later modelled by Ramlow and colleagues in Ref. [78], where they used a network based on an empirical human brain connectivity matrix and FitzHugh-Nagumo oscillators to model the activity of different brain areas. Furthermore, in 2016, Andrzejak and coauthors found strong analogies between chimera states collapses and epileptic seizures [6]. In this study they showed how the collapse of a chimera state in a network of phase oscillators was

preceded by a drop of coherence in the dynamics, and something very similar happens at the onset of an epileptic seizure. In 2018, Chouzouris and colleagues were able to model epileptic seizures by tuning the coupling strength in a network of FitzHugh-Nagumo oscillators with an empirical connectivity obtained from magnetic resonance images of human brains [22]. A recent study from Bansal et al. showed how the interactions of different brain regions during the performance of cognitive tasks give rise to partial synchronization patterns that can be interpreted in the framework of chimera states [10]. Partial synchronization patterns similar to chimera states can also be found in a study on C. elegans by Pournaki et al. [75]. But neuroscience is not the only field in which chimera states are investigated. Studies have shown that these partial synchronization patterns appear also in social systems [31, 44], ecology [9, 45], and models of quantum systems [11]. Efforts to create chimera states in the laboratory gave positive results using different structures and materials. In 2012, Hagerstrom and colleagues observed chimera states in coupled-map lattices [33]. The study combined numerical simulations on chimeras in networks of time-discrete maps and the results obtained using an apparatus that produces an optical nonlinearity in a spatially extended optical system. Another remarkable experiment is the one performed by Martens and colleagues [58]. They took two sets of metronomes and positioned each set on a swing. The two swings were connected via a spring. Modifying the coupling strength between the swings, the system went through different synchronization scenarios, and in particular one in which one population of metronomes is synchronized and the other is asynchronous, which is a chimera state. Chimeras do not only live in physics labs, but also in chemistry labs. Observing chemical oscillators, scientists found that also there partial synchronization appears [99, 100, 102]. In the study [100], Totz and colleagues observed spiral patterns in large populations of non-

locally coupled Belousov-Zhabotinsky chemical oscillators. The core of the spiral is incoherent while the spiral waves are coherent, forming a two-dimensional chimera state.

An important question arises on the road to the observation of chimeras in the physical world and towards their technological applications: is it possible to control chimera states? This issue is a crucial one, since it was proven that chimera states are unstable, and their instabilities become more and more pronounced as one considers smaller systems, which are the most relevant in experimental situations. In general the relative position of the two complementary groups within the network strongly depends on the initial conditions. Furthermore, in small networks, the incoherent group of the chimera state (or equivalently, the coherent group) drifts along the network showing a Brownian motion of its position [72]. Bick and Martens, in Ref. [13], state that the location of the coherent group may have a functional significance, and they envision the possibility of constructing a digital chimera computer where location encondes information. In addition to their drifting along the network, another feature of chimera states that makes them difficult to observe is that in finite-size systems they are chaotic transients [105]. In finite networks of nonlocally coupled oscillators, chimeras coexist with the fully synchronous state. Although in some systems chimeras have a long lifetime, they eventually collapse to the fully synchronous state, which is stable [105]. The properties of this tendency to collapse to full synchronization were extensively investigated in Ref. [6, 105]. Finding ways to prevent this collapse and prolong the chimera's lifetime is one of the goals of control studies.

Methods to achieve control of chimera states have been implemented in models featuring different types of oscillators. In 2014, Sieber and coworkers published a closed-loop method for ring-shaped networks of phase oscillators which used a time-dependent

phase-lag parameter to prevent chimera states from collapsing to the synchronized state [96]. Another closed-loop method based on a gradient dynamics which allows one to maintain the position of the chimera state was proposed by Bick and Martens in 2015 [13]. In 2016, Omelchenko et al. [68] developed a feedback control mechanism, called tweezers, to control chimera states in small networks of FitzHugh-Nagumo and van der Pol oscillators. This method uses two components, a symmetric one to prevent the collapse of chimeras and an asymmetric one to control their position [68]. The tweezers mechanism was optimized in Ref. [66] allowing one to control the size of the domains forming the chimera state and the frequency difference among the oscillators in each domain. Gambuzza and Frasca [25] used spatial pinning to control the position of chimera states in networks of FitzHugh-Nagumo and phase oscillators. Isele and collaborators conducted a study about control of the position of chimeras in networks of oscillatory FitzHugh-Nagumo units [38]. They introduced a barrier of excitable units in the network, which attracts the incoherent region [38]. In the work by Andrzejak et al. [6], closed-loop feedback control schemes were used to suppress or promote the collapse of the chimera to the synchronous state in networks of phase oscillators. Recently, the possibility of controlling some features of chimera states in networks of Stuart-Landau oscillators acting on the initial conditions and coupling scheme has been developed by Kalle and collaborators [39]. It was also proven that it is possible to control not only classical phase chimeras, but also amplitude chimeras which are observed in networks of Stuart-Landau oscillators [30]. Furthermore, in phase oscillator networks with coupling functions involving higher order harmonics, chimera states can be stabilized without external influence [14, 98]. In contrast to this variety of methods for single-layer networks, control of chimera states in multilayer networks is still widely unexplored. In 2019,

Omelchenko and coauthors showed that the tweezers control mechanism introduced in [68] can also be used to control chimera states in multiplex networks of van der Pol oscillators [63].

The studies mentioned so far on control of chimeras rely on modifications of parameters of the oscillators and in some cases these changes are made according to information extracted from the system in a closed loop. However, in real-world scenarios, it might be difficult to alter the individual oscillators that form a network. Closed-loop feedback methods could also result unreliable, for example when measurements of system features are affected by noise.

In this thesis we propose a new control method based on the idea of a pacemaker oscillator [82, 83]. This is an oscillator that does not receive any input from other nodes of the network but sends information to them, and therefore it oscillates at a constant frequency. This method is implemented by modifying only the connectivity structure of the network. Therefore, it does not require one to act on individual oscillators, nor to retrieve any feedback from the system. These characteristics make it appealing for possible experimental applications. In what follows, we first introduce the pacemaker mechanism in single-layer networks of phase oscillators and we analyze its effects on the drifting and collapse. Furthermore, we generalize the idea of a pacemaker oscillator to investigate which is the minimal modification of the network connectivity needed to control chimeras. Secondly, we study the applicability of this mechanism in multiplex networks of phase oscillators and oscillatory FitzHugh-Nagumo neuron models. In the analysis, we use classical tools introduced to characterize chimera states and we develop new measures to assess the effectiveness of our control mechanism.

CHAPTER 2

Chimera states

In this chapter we introduce the basic concepts about chimera states in networks of phase oscillators and FitzHugh-Nagumo oscillators which are of fundamental importance for all the subsequent chapters of this thesis. We describe how to detect chimera states and how to determine which oscillators are in the coherent and incoherent groups.

2.1 Nonlocal coupling

An essential element to obtain classical chimera states like the ones discovered by Kuramoto [47] is the nonlocal coupling structure in the network. This type of coupling is used in the majority of studies about chimeras states. Nonlocal coupling is the middle point between local and global coupling. Local coupling means that each oscillator is coupled only to its closest neighbours. On

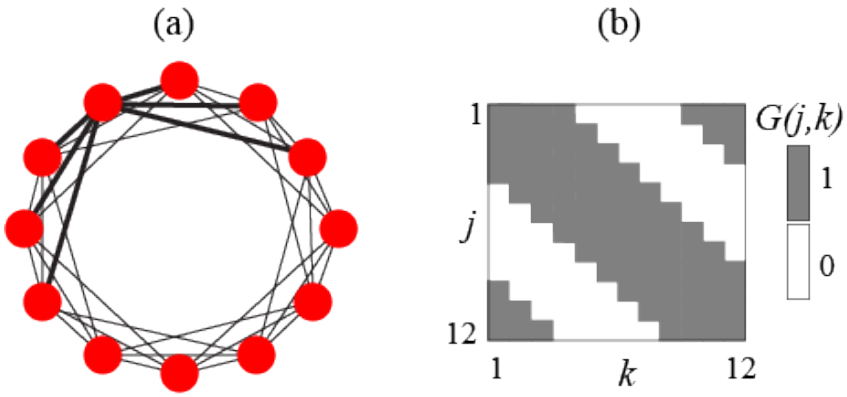

Figure 2.1: Nonlocal coupling. Panel (a) shows a schematic representation of a ring network with nonlocal coupling. In panel (b) we display the connectivity matrix of the network in panel (a). The parameters are $N = 12$ and $R = 3$.

the contrary, global coupling means that each oscillator is coupled to all other oscillators, therefore it can be implemented also in populations and does not imply any spatial ordering. Most of the studies on chimera states use ring-shaped networks, which can also be thought of as chain of oscillators with periodic boundary conditions. In a ring-shaped network, nonlocal coupling is obtained connecting each oscillator to more than one neighbour on each side. A schematic representation of this kind of coupling is given in Figure 2.1(a). Given one oscillator, its links can have all the same strength, or their intensity can decrease with increasing distance from that oscillator. The former case is represented by a regtangular coupling kernel, while the latter by an exponential or sinusoidal coupling kernel. We will consider a rectangular coupling kernel throughout this thesis. The connectivity matrix G for a nonlocally coupled ring-shaped network of N oscillators with a rectangular

coupling kernel has the following mathematical expression:

$$G(j,k) = \begin{cases} 1, \text{ if } |j-k| \leq R, \\ 0, \text{ otherwise} \end{cases} \tag{2.1}$$

Here j, k are spatial indeces with ranges $j, k = 1 \ldots N$, and R is the broadness of the coupling kernel, that is the number of oscillators connected to a given oscillator on each side.

2.2 Phase oscillators

As a first model that can produce chimera states we use a ring network of N nonlocally coupled phase oscillators (see Figure2.1). This network is described by the following system of differential equations for the time-dependent phases $\phi_j(t)$ of the oscillators [72, 105]:

$$\dot{\phi}_j(t) = \omega - \frac{1}{2R} \sum_{k=1}^{N} G(j,k) \sin\left(\phi_j(t) - \phi_k(t) + \alpha\right) \tag{2.2}$$

where $j = 1, \ldots N$. The oscillators' natural frequency ω is set to zero without loss of generality. The connectivity matrix G corresponds to a rectangular coupling kernel with broadness R [72, 105] (see Eq. (2.1)). The phase-lag parameter is set to $\alpha = 1.46$ [105]. Reflecting the periodic boundary conditions of the network's ring shape, all sums and differences of indices are to be understood modulo N. In Figure 2.2 we show two typical solutions for the system of equations (2.2) with parameters $N = 50$, $R = 18$. The system was integrated using the classical 4th order Rung-Kutta algorithm in an interval $I = [t_1, t_n]$ with time steps of width dt, corresponding to $(t_n - t_1 + 1) \cdot dt$ dimensionless time units. The initial conditions were chosen randomly and uniformly distributed

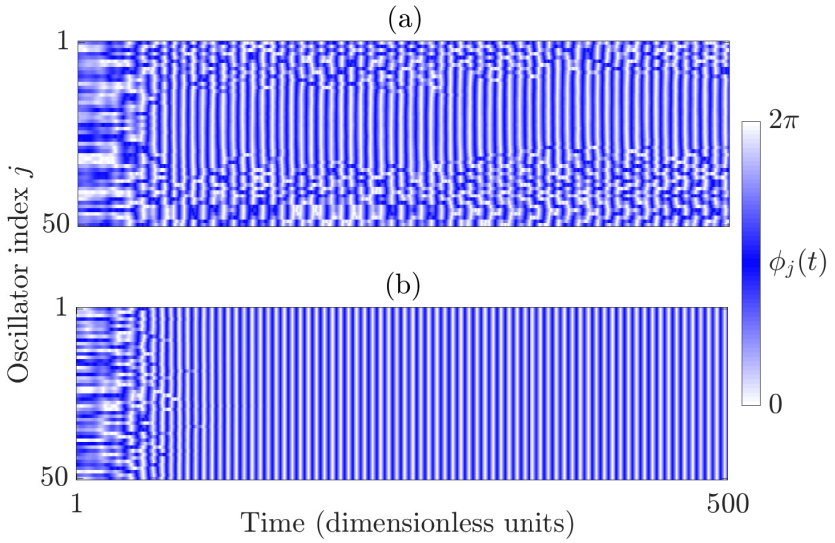

Figure 2.2: Chimera states vs. full synchronization. Two exemplary solutions of Eq. (2.2) for two different initial conditions. We show the spacetime evolutions of the phases $\phi_j(t)$. In panel (a), a chimera state was formed and we can see the two complementary groups. In panel (b), the sytem collapsed almost immediately to the fully synchronous state, without ever forming a chimera state. Network parameters: $N = 50$, $R = 18$, $\alpha = 1.46$. Integration interval $I = [1, 100000]$ and time step $dt = 0.05$.

in the interval $[0, 2\pi)$. In Figure 2.2(a) we see the phase variables $\phi_j(t)$ of a solution in which a chimera state has formed. The two complementary groups are clearly visible, the coherent one showing an almost periodic dynamics and the incoherent one performing an erratic motion. In Figure 2.2(b) we show another possible solution of Eq. (2.2), obtained from different random initial conditions, that is the fully synchronized state, in which, after a short transient, all oscillators perform a synchronous motion.

Apart from the display of the phases such as the one in Figure 2.2, chimera states can be visualized by means of their in-

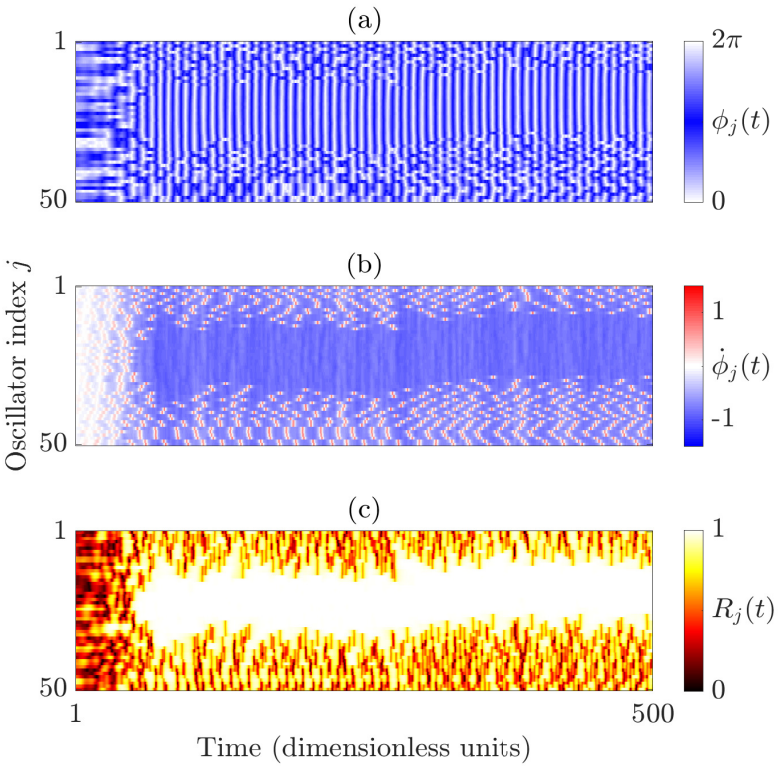

Figure 2.3: Different representations of a chimera state. In panel (a) we replicate the chimera state of Figure 2.2(a). Panel (b) shows the instantaneous phase velocities $\dot{\phi}_j(t)$ and panel (c) the local order parameter $R_j(t)$. All parameters are the same as in Figure 2.2.

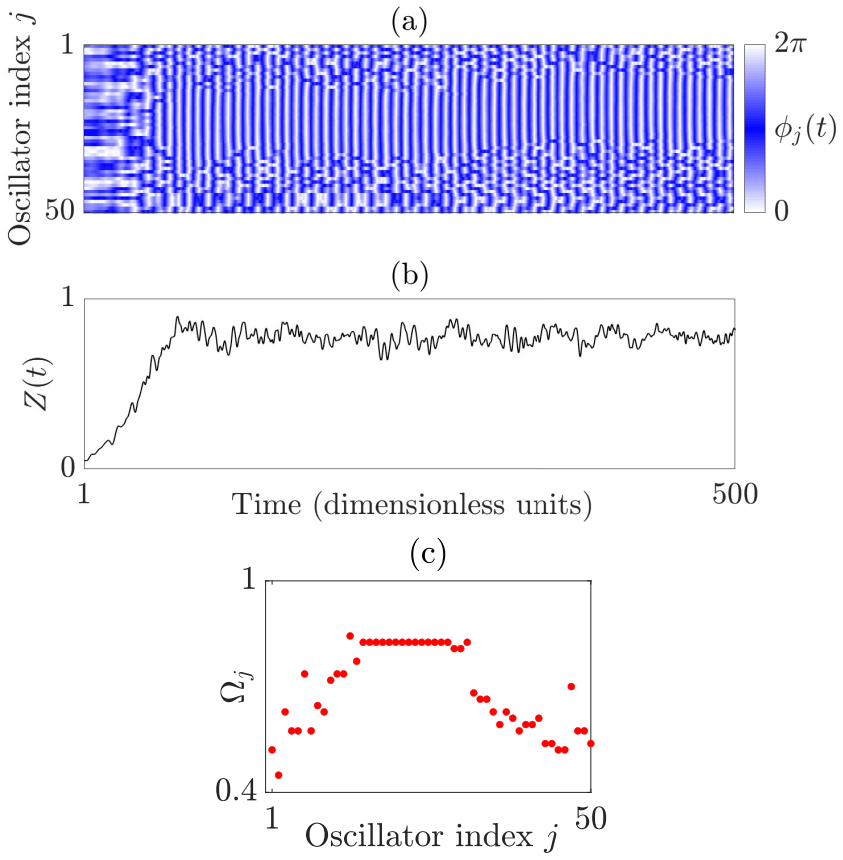

Figure 2.4: Order parameter and mean phase velocity. Panel (a) shows a chimera states and panel (b) its order parameter $Z(t)$. Panel (c) and shows the chimera's mean phase velocity profile Ω_j in a time window W of 100 dimensionless units starting at $t = 200$. All parameters are the same as in Figure 2.2.

stantaneous phase velocities or local order parameter. From the phases displayed in Figure 2.2(a), (b) we can calculate these local quantities useful to characterize the different dynamical regimes. The instantaneous phase velocities are defined as follows for $j = 1, \ldots, N$:

$$\dot{\phi}_j(t) = \frac{\phi_j(t) - \phi_j(t-1)}{dt}. \tag{2.3}$$

The local order parameter measures the local degree of coherence of one oscillator with its δ neighbours on each side and it is defined as:

$$Z_j(t) = \left| \frac{1}{2\delta + 1} \sum_{|k-j| \leq \delta} e^{i\phi_k(t)} \right|. \tag{2.4}$$

Figure 2.3(b) shows the spacetime evolution of the instantaneous phase velocities $\dot{\phi}_j$. We see an irregular pattern corresponding to the incoherent group and a region of almost uniform colour corresponding to the coherent region of the chimera. The range of $Z_j(t)$ is the interval $[0, 1]$, where a value of 1 corresponds to full synchrony and 0 to complete incoherence. For the local order parameter $Z_j(t)$ in Figure 2.3(c), we see a uniform part with values of $Z_j(t)$ close to 1 corresponding to the coherent group and an irregular pattern with values $Z_j(t) < 1$ for the incoherent group.

The local order parameter can be generalized to measure the degree of coherence of the whole network calculating the following quantity $Z(t)$, known simply as order parameter:

$$Z(t) = \left| \frac{1}{N} \sum_{k=1}^{N} e^{i\phi_k(t)} \right| \tag{2.5}$$

In Figure 2.4(b) we show the typical behaviour for the order parameter $Z(t)$ of a chimera state. During the short initial transient which leads to the chimera's formation, $Z(t)$ increases rapidly and

subsequently it oscillates around a mean value of approximately 0.75.

Another quantity that characterizes the spatial profile of a chimera state is the mean phase velocity Ω_j, calculated in a time window $W \subset I$:

$$\Omega_j = \left\langle \dot{\phi}_j(t) \right\rangle_W \tag{2.6}$$

where $j = 1 \ldots N$ and $\langle\ \rangle$ is the time average over the window W. Figure 2.4(c) shows the profile of the chimera's mean phase velocity calculated in a time window W of 100 dimensionless units of the solutions shown in Figure2.4(a). The constant part of Ω_j corresponds to the coherent group.

2.2.1 Detection of chimera states

The content of this section was adapted from Appendix A of G. Ruzzene, I. Omelchenko, E. Schöll, A. Zakharova, R. G. Andrzejak, *Controlling chimera states with minimal coupling modifications*, Chaos: an interdisciplinary journal of nonlinear science, 29, 051103 (2019) [82].

The algorithm used in this thesis to detect chimera states is an adaptation of the one proposed in Ref. [38]. We integrate Equation (2.2) to obtain a solution $\phi_j(t)$, then we calculate the Kuramoto global order parameter $Z(t)$ and compute its temporal average $Z = \langle Z(t) \rangle_W$ over a time window W located at the end of the integration interval I. We compute the mean phase velocities Ω_j in the same time window W and we determine the range of the mean phase velocity profile [3]:

$$\Omega = \max_{j=1,\ldots,N} \Omega_j - \min_{j=1,\ldots,N} \Omega_j. \tag{2.7}$$

If we find that $Z \in [0.65, 0.8]$ and $\Omega \in [0.1, 1]$ then the solution $\phi_j(t)$ is classified as a chimera state. All of these threshold values

were chosen after pre-analysis of the considered system. The other possible scenarios for Equation 2.2 are solutions which are completely incoherent and solutions in which the oscillators are all synchronized or almost all synchronized. The former are discarded by the lower bound on the order parameter. The latter are also ruled out because $Z = 1$ if all oscillators are synchronized. The condition on the mean phase velocity comes into play when we have values of Z close to 0.65. There are some cases in qhich there is no clear distinction between the coherent and incoherent group and $\Omega < 0.1$. The upper-bound for Ω discards situations that are rarely observed in presence of high coupling, in which a chimera state is not formed but the synchronized state is disturbed by few oscillators that have a different frequency from the synchronized block.

2.2.2 High- and Low-Coherence groups

The content of this section was adapted from Appendix B of G. Ruzzene, I. Omelchenko, E. Schöll, A. Zakharova, R. G. Andrzejak, *Controlling chimera states with minimal coupling modifications*, Chaos: an interdisciplinary journal of nonlinear science, 29, 051103 (2019) [82].

Following the terminology introduced in [6], we refer to the two complementary groups that form the chimera states as the high coherence group (HCG) and low coherence group (LCG). These two groups are defined following the algorithm presented in Ref. [6]. In what follows all indices and sums of indices are to be understood modulo N. For the j-th oscillator we consider its two nearest neighbors on each side, that is oscillators $j-2, j-1, j+1, j+2$. For every time instant t we calculate the pairwise local

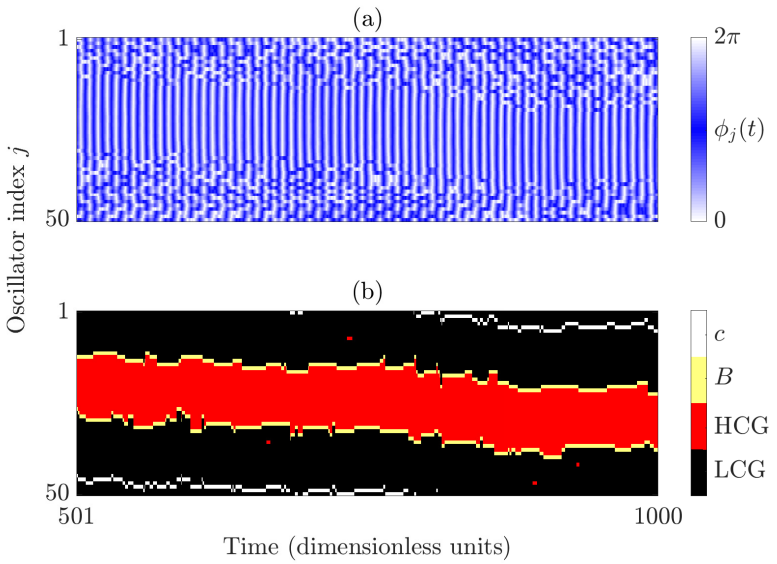

Figure 2.5: Center of the chimera's low coherence group. Panel (a) is the temporal evolution of the phases $\phi_j(t)$ of a chimera state,o and panel (b) represents the positions of its different compnents: the LCG (black), the HCG (red), the border $B(t)$ between HCG and LCG (yellow) and the center $c(t)$ of the incoherent group (white). All parameters are the same as in Figure 2.2.

order parameters:

$$Z_{j_1,j_2}(t) = \left| \frac{1}{2} \left(e^{i\phi_{j_1}(t)} + e^{i\phi_{j_2}(t)} \right) \right|. \tag{2.8}$$

We define the following function:

$$\chi(j,t) = \begin{cases} 1 \text{ if } Z_{j+2,j+1}(t), Z_{j+1,j}(t), \\ \qquad Z_{j,j-1}(t) \text{ and } Z_{j-1,j-2}(t) > 0.995, \\ 0 \text{ otherwise.} \end{cases} \tag{2.9}$$

At time t the HCG is formed by all oscillators with indices j such that $\chi(j,t) = 1$. The LCG is formed by the remaining oscillators. Once we defined the HCG and LCG, we can define the border of the LCG and its center. Descarding the initial transients during which the chimera is formed, for every t we look for indices k_B, j_B which satisfy the following conditions:

$$\begin{aligned} &\chi(k_B - 1, t) = 1 \text{ and } \chi(k_B, t) = \chi(k_B + 1, t) = 0 \\ &\chi(j_B - 1, t) = \chi(j_B, t) = 0 \text{ and } \chi(j_B + 1, t) = 1 \end{aligned} \tag{2.10}$$

If such indices exist we say that the border of the LCG is $B(t) = \{k_B, j_B\}$. Apart from the main LCG, it may happen that there are small islands of incoherent oscillators inside the HCG. In this case we find multiple pairs of indices satisfying the conditions above. We then choose the pair which corresponds to the biggest incoherent group. The position $c(t)$ of the center of the LCG at time t is defined according to the following rule:

- if $k_B < j_B$ then $c(t) = \frac{k_B + j_B}{2}$;
- if $k_B > j_B$ then $c(t) = \frac{k_B + j_B + N}{2} \bmod N$.

The center position $c(t)$ defined above can be an integer or half-integer between 0.5 and the network size N. The size of the LCG at

time t is $s(t) = N - \sum_{k=1}^{N} \chi(k,t)$. Figure 2.5 illustrates the results obtained applying the algorithms in this subsection to the chimera state shown in panel (a). The position of the center of the LCG will be one of the main subjects of interest in the next chapters.

2.3 FitzHugh-Nagumo oscillators

The FitzHugh-Nagumo model [23, 61] is a two-dimensional simplification of the Hodgkin-Huxley model [37], which descibes spike generation by neurons. The equation of one isolated FitzHugh-Nagumo unit can be written as follows [50]:

$$\begin{aligned} \varepsilon \frac{du(t)}{dt} &= u - \frac{u(t)^3}{3} - v(t) \\ \frac{dv(t)}{dt} &= u(t) + a. \end{aligned} \tag{2.11}$$

Here, u is the activator variable that describes the neuron's membrane potential, and v is the inhibitor variable. The parameter $\varepsilon \ll 1$ provides a time-scale separation between the two variables. Throughout this thesis, we will set $\varepsilon = 0.05$. Therefore, u is a fast variable while v is a slow variable. The parameter a is a bifurcation parameter which determines whether the neuron is excitable ($a > 1$) or oscillatory ($a < 1$). The FitzHugh-Nagumo model gives a qualitative description of a neuron's spiking activity. In this thesis we will consider only oscillatory FitzHugh-Nagumo units, by setting the bifurcation parameter $a = 0.5$. The temporal evolution of the two variables u and v in Eq. (2.11) is shown in Figure 2.6(a). In Figure 2.6(b) one can see the characteristic phase portrait of an individual FitzHugh-Nagumo unit and its nullclines.

In analogy with the setting described for phase oscillators in Section 2.2, we use a ring-shaped network of nonlocally coupled FitzHugh-Nagumo oscillators. The dynamics of this network is

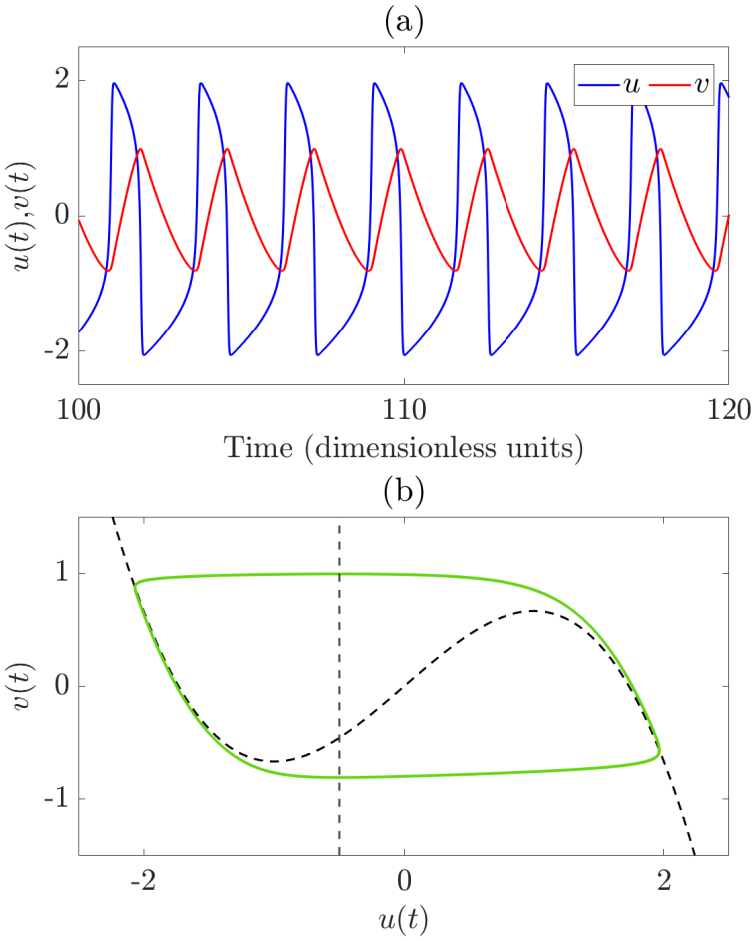

Figure 2.6: Dynamics of an isolated FitzHugh-Nagumo neuron. Panel (a) shows the temporal evolution of variables $u(t)$ (blue) and $v(t)$ (red). Panel (b) shows the corresponding phase portrait (green) and the nullclines of Eq. (2.11) (dashed black).

governed by the following set of differential equations [69]:

$$\begin{aligned}
\varepsilon\frac{du_j(t)}{dt} &= u_j(t) - \frac{u_j(t)^3}{3} - v_j(t) \\
&\quad + \frac{\sigma}{2R}\sum_{k=j-R}^{j+R}\left[b_{uu}(u_k(t)-u_j(t)) + b_{uv}(v_k(t)-v_j(t))\right] \\
\frac{dv_j(t)}{dt} &= u_j(t) + a_j \\
&\quad + \frac{\sigma}{2R}\sum_{k=j-R}^{j+R}\left[b_{vu}(u_k(t)-u_j(t)) + b_{vv}(v_k(t)-v_j(t))\right]
\end{aligned} \tag{2.12}$$

Here, $j = 1 \ldots N$ and σ is the coupling strength and R is the broadness of the rectangular coupling kernel. The coupling is obtained using a rotational matrix:

$$\begin{pmatrix} b_{uu} & b_{uv} \\ b_{vu} & b_{vv} \end{pmatrix} = \begin{pmatrix} \cos\theta & \sin\theta \\ -\sin\theta & \cos\theta \end{pmatrix} \tag{2.13}$$

It was shown in Ref. [69] that for θ slightly smaller than $\pi/2$ this system can sustain chimera states. Therefore, throughout this thesis we will set $\theta = \pi/2 - 0.1$. Also the coupling strength σ plays an important role in the formation of chimera states in this model. We will always choose $\sigma \in [0.1, 0.2]$ [59, 69]. We again use the classical 4th order Runge-Kutta algorithm to integrate this system during an integration interval I with time step dt.

To extract a phase $\phi_j(t)$ from the variables $u_j(t)$ and $v_j(t)$ we use [69]:

$$\phi_j(t) = \arctan\frac{u_j(t)}{v_j(t)}. \tag{2.14}$$

In Figure 2.7(a) we display a chimera state obtained from the

model in Eq. (2.12) by showing the spatiotemporal evolution of the activator variables $u_j(t)$, including the initial formation. In Figure 2.7(b) we show the phases of the same chimera state.

Once we extract phases from the variables of FitzHugh-Nagumo oscillators we can calculate all the quantities introduced in the previous section for phase oscillators. Specifically, we can define local and global order parameters Z_j and Z (Eqs. (2.2) and (2.5)), and the mean phase velocity Ω_j (Eq. (2.6)). We also apply the same algorithms for chimera detection (Section 2.2.1) and to compute the HCG, the LCG and its center (Section 2.2.2).

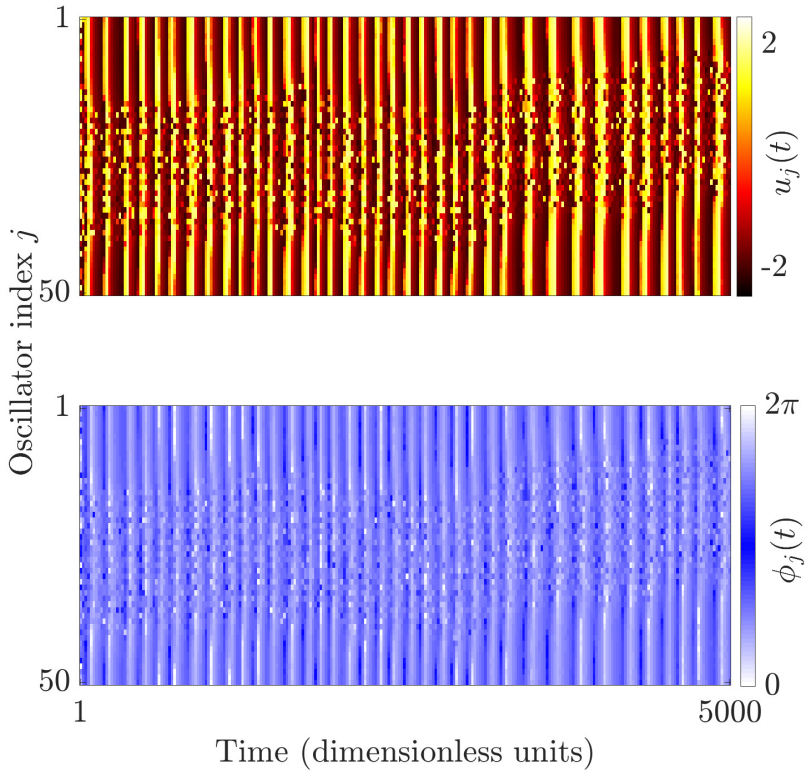

Figure 2.7: A chimera state in a network of FitzHugh-Nagumo oscillator. Network parameters: $N = 50$, $R = 18$, $\sigma = 0.2$. Integration interval $I = [1, 500000]$ with a time step $dt = 0.01$.

CHAPTER 3

Control of chimera states in networks of nonlocally coupled phase oscillators

The content of this chapter was adpted from: G. Ruzzene, I. Omelchenko, E. Schöll, A. Zakharova, R. G. Andrzejak, *Controlling chimera states with minimal coupling modifications*, Chaos: an interdisciplinary journal of nonlinear science, 29, 051103 (2019) [82].

In this chapter we introduce the main idea of this thesis: a control method for chimera states based on a pacemaker oscillator. The first model we consider to define the control and study its effects is a ring-shaped network of phase oscillators. This model was defined in Section 2.2. The phase variables $\phi_j(t)$ evolve according to Eq. (2.2). In Figure 3.1 we show three realizions of this model which illustrate the instabilities of chimera states that we will control. The first one, Figure 3.1(a), is a chimera state, and we see that the two complementary groups drift along the network [72]. In the second realization, a chimera state is formed and its groups drift along the

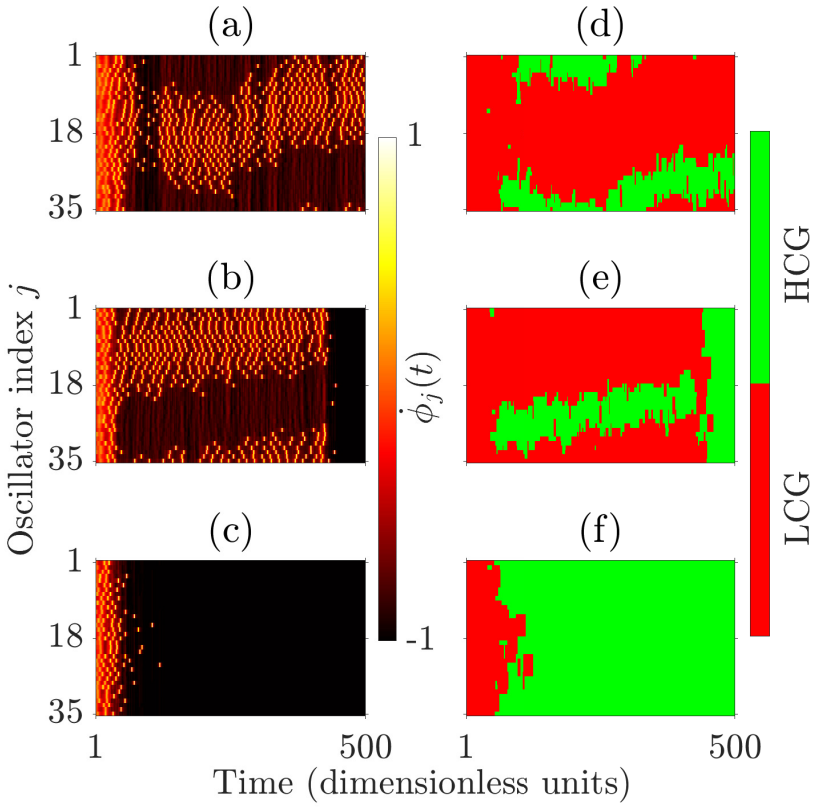

Figure 3.1: Uncontrolled chimera states drift along the network over time and may collapse to the fully synchronous state. In panels (a), (b), (c), we display instantaneous phase velocities $\dot{\phi}_j(t)$ for three different realizations of Eq. (2.2) for $N = 35, R = 12$, $\alpha = 1.46$, $\omega = 0$. (a) Chimera state, (b) chimera state collapses, (c) chimera state is never formed. Panels (d), (e), (f) illustrate the corresponding representations of the high coherence group (HCG) and the low coherence group (LCG) obtained using the algortihm described in Section 2.2.2.

network, but the chimera collapses before the end of the simulation (Figure 3.1(b)). In Figure 3.1(c) we display the last realization, in which a chimera does not form, but instead all of the oscillators synchronize after a short initial transient. The collapse of chimeras to the fully synchronized state in finite-size systems was studied in Refs. [6, 105]. To analyze the effects of our control mechanism we need to be able to characterize the chimera's high coherence and low coherence groups (HCG and LCG). In Figure 3.1(d),(e),(f) we show a binary representations of the groups corresponding to the solutions in panels (a), (b) and (c) respectively. These were obtained using the algorithm described in Section 2.2.2.

3.1 Modifying network connectivity to control chimeras

Our control mechanism acts on the connectivity matrix G defined in Chapter 2 in Eq. (2.1). We implement the idea of a pacemaker oscillator in the model in the following way. We decide to have the pacemaker in position p, which corresponds to setting to zero all nondiagonal elements of the p-th row of G. Accordingly, the p-th oscillator does not receive any input and as a consequence it oscillates at a constant angular frequency $\dot{\phi}_p(t) = -\sin(\alpha)$. However, since the p-th column of G is maintained, this constant frequency is received by all oscillators within the coupling range R of oscillator p (see Figure 3.2, panels (b), (d)). In Figure 3.3 we show the effects of the pacemaker which we found in this thesis: attracting the low coherence group and preventing the collapse to the synchronized state. In panels (d), (e), (f) we start the system with the same initial conditions as in panels (a), (b), (c) respectively, but now a pacemaker is present in position $p = 18$. We see how the pacemaker attracts the low coherence groups and in both panels (e)

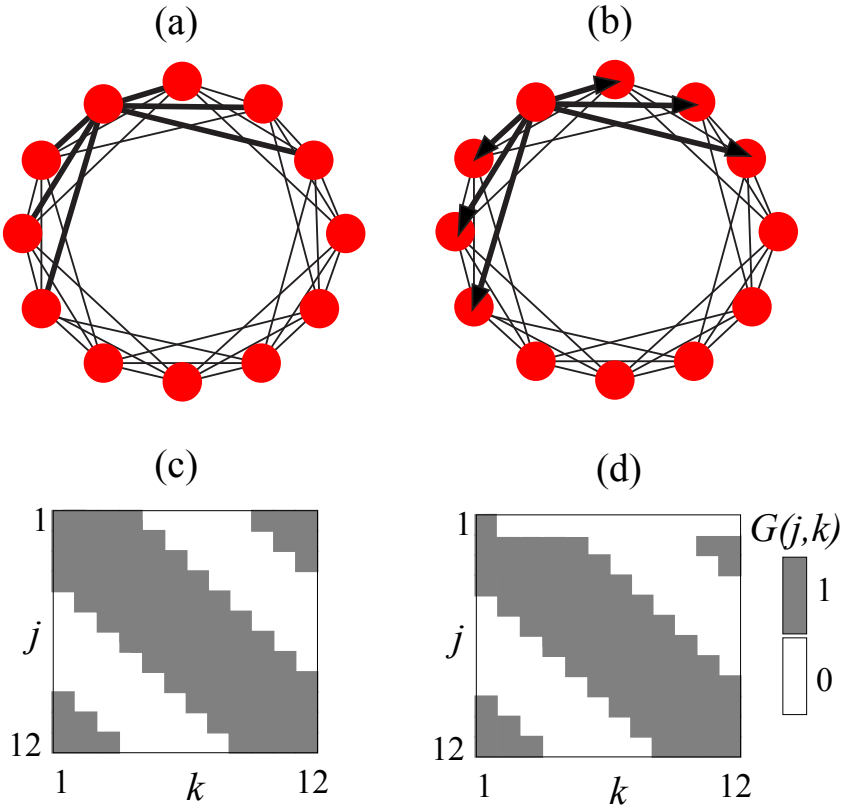

Figure 3.2: Implementation of the full pacemaker in position $p = 1$. In panel (a) we show a network of 12 oscillators which are nonlocally coupled with $R = 3$. The links of one oscillator are highlighted to better show the nonlocal coupling configuration. In panel (b) we show how we change the connectivity to implement the pacemaker: we choose one oscillator (the one with highlighted links in panel (a)) and we make its link unidirectional. The corresponding coupling matrices $G(j, k)$ are shown in panels (c) and (d) respectively.

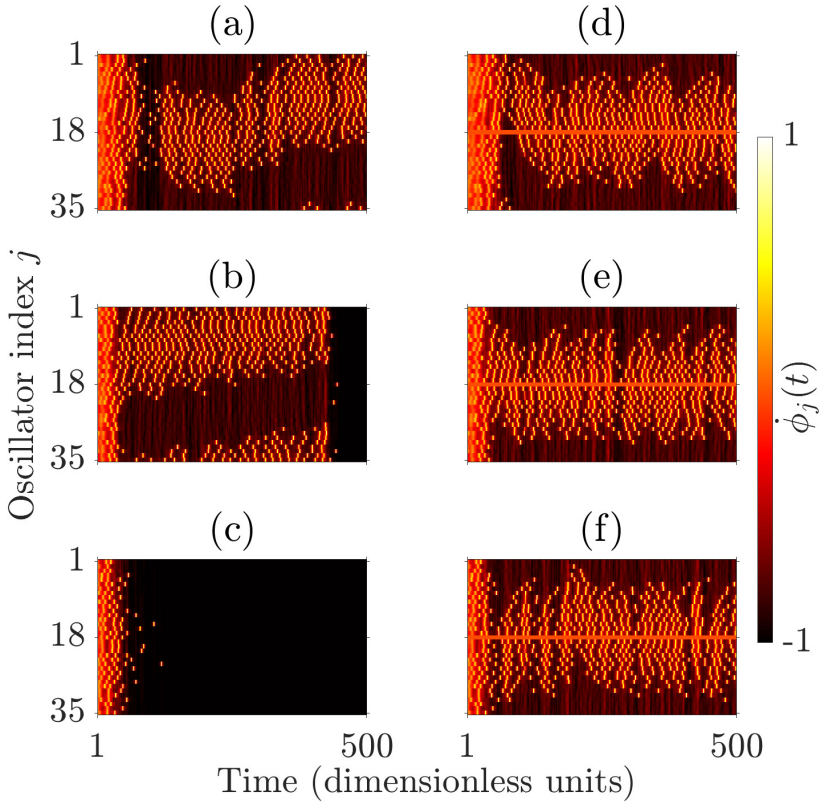

Figure 3.3: A pacemaker prevents the chimera's drifting and collapse. (a), (b), (c) are replicas from Figure 3.1(a), (b), (c). In panels (d), (e), (f) we display the effects of the presence of a pacemaker in position 18 on the solutions shown in panels (a), (b), (c) respectively. The pacemaker was activated at the beginning of the simulations. The constant frequency of the pacemaker appears as a uniform stripe in line 18 of panels (d), (e), (f).

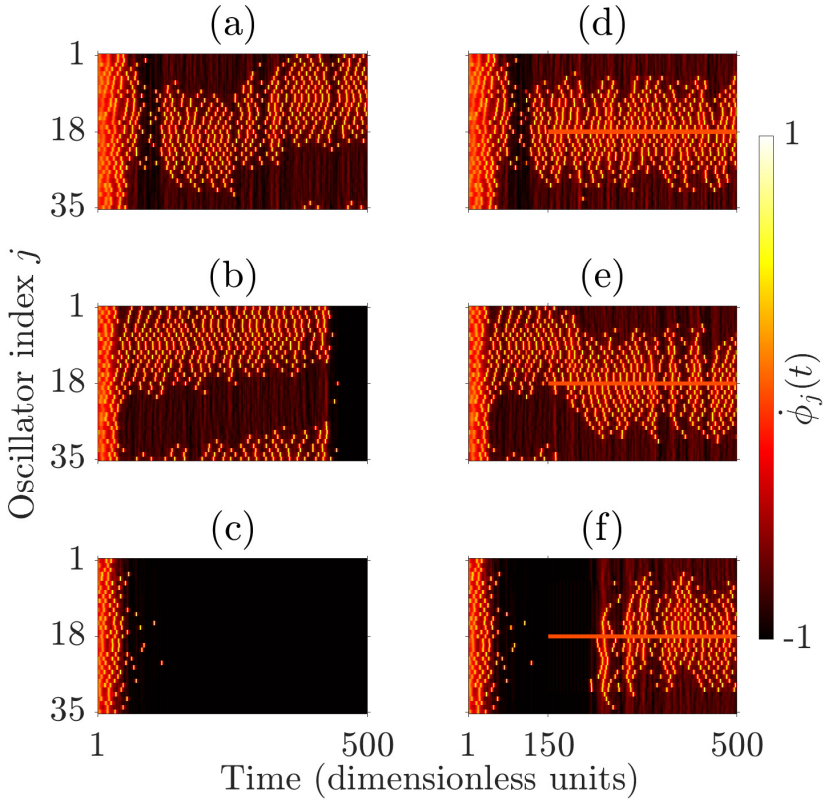

Figure 3.4: A pacemaker generates chimera states. (a),(b),(c) are replicas from Figure 3.1(a),(b),(c). Panels (d), (e), (f) are analogous to the same panels in Figure 3.3 but here the pacemaker was activated after 150 dimensionless time units.

and (f) the collapse to the synchronous state is avoided. In Figure 3.4, we see how the same effects are obtained when we activate the pacemaker after a certain time from the beginning of the simulation. The pacemaker attracts the LCG in all simulations and it does not only prevent the collapse in Figure 3.4(e), but it can also trigger the formation of a chimera from the synchronous state in Figure 3.4(f).

After studying the effects of this full pacemaker, we implement gradually less invasive modifications of the coupling matrix G. Like we just described, in the pacemaker configuration, only the diagonal element is maintained at $G(p,p) = 1$. Starting from this most invasive control, we then restore the pair of first off-diagonal elements $G(p,p-1) = G(p,p+1) = 1$, then the pair of second off-diagonal elements $G(p,p-2) = G(p,p+2) = 1$, etc. This process is continued until we set the elements $G(p,p-R+1) = G(p,p+R-1) = 1$. Therefore, at this stage only the elements $G(p,p-R), G(p,p+R)$ remain modified to zero. We refer to the case in which all coefficients of the p-th row of G are set to zero as *full pacemaker* (Figure 3.2 (b), (d)), and to the intermediate modifications of G described above as *partial pacemaker*. The *pacemaker intensity* ψ is defined as the ratio between the number of removed links and the initial number of bidirectional connections of the pacemaker. The lowest possible nonzero value of ψ is $1/R$, which corresponds to just two unidirectional links of oscillator p. Finally, we set $G(p,p-R) = 1$ and $G(p,p+R) = \xi$, where ξ is varied form 0 to 1. That means, for $\xi = 1$ the unchanged connectivity matrix G is restored (see Eq. (2.1)).

3.2 Triggering chimera states

In this section we demonstrate how we can use a pacemaker to induce chimera states for parameters and initial conditions for which they do not form spontaneously (see again Figure 3.3, panels

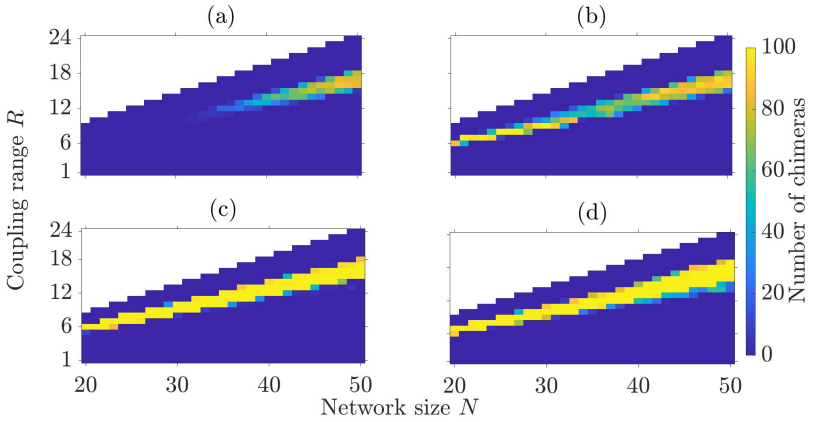

Figure 3.5: A pacemaker triggers chimeras for initial conditions for which they do not form spontaneously. Comparison of the number of chimera states observed for different values of the network size N and coupling broadness R (the other network parameters are $\alpha = 1.46$, $\omega = 0$). For each pair of values we solved the model 100 times without control (panel (a), $\psi = 0$), with low control intensity $\psi = \frac{1}{R}$ (panel (b)), intermediate control intensity $\psi \approx 0.5$ (panel (c)) and with a full pacemaker corresponding to $\psi = 1$ (panel (d)).

(e), (f)). We compare the percentage of chimeras obtained with different pacemaker intensities ψ and for every pacemaker intensity we use the same set of initial conditions. It is known that the lifetime of chimeras increases with the number of oscillators N (Ref. [105]) and the drifting increases with decreasing N [72]. Since our control aims to counteract these instabilities, we focus on small networks of up to $N = 50$, and we insert a pacemaker in position $p = 1$ of the network. To detect chimeras we use the algorithm described in Section 2.2.1. For each value of the network size we consider all the possible values of coupling range R varying from local coupling $R = 1$ to global coupling $R = \frac{N-1}{2}$ when N is odd, or from $R = 1$ to the maximum possible value $R = \frac{N-2}{2}$ when N is even. For this section, the integration was performed over $4 \cdot 10^5$ sampling times, corresponding to $2 \cdot 10^4$ dimensionless time units, and all analyses were performed over an evaluation interval of 2500 dimensionless time units $W = [17500,\ 20000]$. We considered 100 independent realizations for all pairs of values of network size N and coupling range R. Results are displayed in Figure 3.5. We clearly see that the region of the parameter space in which chimeras are detected is broader when a pacemaker is present in the network (see Figure 3.5 (b), (c), (d)). When no control is applied to the network (Figure 3.5 (a)), no chimeras are found for $N < 32$ and for relative coupling range R/N outside the interval $[0.25, 0.4]$. This is due to the presence of chimera states whose lifetime is shorter than the integration time (Figure 3.1(c)) and to initial conditions that collapse immediately to the synchronous state without ever forming a chimera state (see again Figure 3.1(b)). In the region where chimera states are present for the unchanged connectivity (Figure 3.5 (a)) we observe an increase in their percentage when the pacemaker is present (Figure 3.5 (b),(c),(d)). In particular, a low intensity pacemaker with $\psi = 0.06$, obtained cutting only two incoming links, already induces chimeras

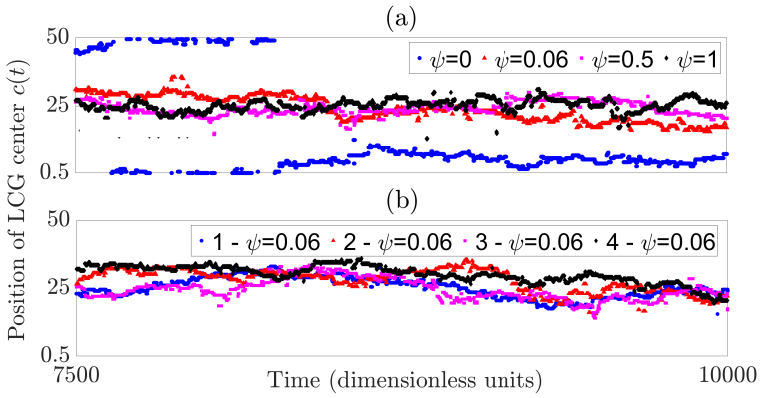

Figure 3.6: The center $c(t)$ of the LCG is attracted by a pacemaker with different intensities. Panel (a) is the temporal evolution of the center of the LCG for the same realization of Eq. (2.2) with different pacemaker intensities, starting with no control up to the full pacemaker. In panel (b) we show four independent realizations of Eq. (2.2) with low pacemaker intensity. The pacemaker is in position $p = 25$.

for small values of $N < 32$ (see Figure 3.5 (b)). For pacemaker intensity $\psi \approx 0.5$ (panel (c)) we obtain results that are close to the case of the full pacemaker (panel (d)).

3.3 Controlling the position of chimeras

Our study proceeds with the control of the position of chimera states. In Figure 3.1 (a) we already saw that the two complementary groups LCG and HCG drift along the network [72]. This drifting is particularly pronounced for small networks and it was characterized as a Brownian motion [72]. We study how different pacemaker intensities ψ affect the chimera's position. To do this, we set $N = 50$ and $R = 18$. For these parameters the occurrence of chimera states is more likely in comparison with smaller sizes N, while the drifting of the LCG and HCG is still substantial. The pacemaker

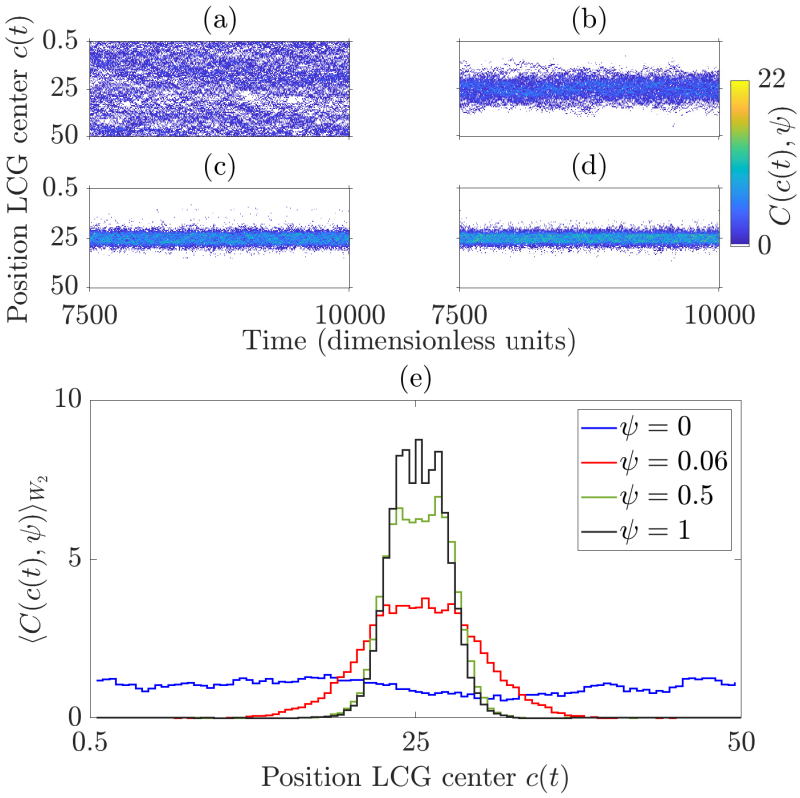

Figure 3.7: Gradually cutting incoming links of one oscillator allows one to increasingly control the position of the chimera state. We show the effects on chimera states of the presence of a partial/full pacemaker in position $p = 25$, in a network with $N = 50$, $R = 18$, $\alpha = 1.46$. The color scale in panels (a), (b), (c), (d) represents values of the distributions of the LCG center $C(c(t), \psi)$ over 100 independent realizations. Panel (a) shows how the center $c(t)$ of the LCG is positioned without any control, that is with an unmodified matrix G. In (b) the pacemaker intensity is $\psi = 0.06$, while in (c) we have $\psi = 0.5$. In panel (d) the configuration corresponding to the full pacemaker, i.e. $\psi = 1$ is displayed. In panel (e) we show the corresponding time averages of the spatial distributions $C(c(t), \psi)$ of the LCG center position over the interval W_2.

is in position $p = 25$. For this section, integration was performed over $2 \cdot 10^5$ sampling times, corresponding to 10^4 dimensionless time units, and all analyses were performed over an evaluation interval of 2500 dimensionless time units $W_2 = [7500, 10000]$. Following Ref. [5], if at some point the system synchronized, we started over with new initial conditions. For every time step t we define the position of the center of the LCG, denoted by $c(t)$, following the algorithm in Chapter 2, Section 2.2.2. The values of $c(t)$ vary in the set $\mathcal{L}$ of numbers from 0.5 to $N = 50$ in steps of 0.5. Furthermore, we calculate the size $s(t)$ of the LCG and the distance $d(t) = c(t) - 25$ of its center from the pacemaker position $p = 25$ (see Section 2.2.2). In Figure 3.6 (a) we show the temporal evolution of the position of the center $c(t)$ of the LCG for four solutions of Eq. (2.2) corresponding to four different pacemaker intensities $\psi = 0,\ 0.06,\ 0.5,\ 1$, where $0.06 \approx \frac{1}{R}$. The initial conditions were the same in every realization. In panel (b) we show four different realizations of Eq. (2.2) with low pacemaker intensity $\psi = 0.06$. This is the lowest possible value in our setting, as it corresponds to only two unidirectional links. In both panels one can appreciate the attracting effect of the pacemaker on the center of the LCG. In the presence of a pacemaker, even with low intensity, the center of the LCG is attracted by the pacemaker, as it becomes evident from the difference in the characteristics of the blue to the red curve in Figure 3.6 (a). The control effect becomes stronger for increasing pacemaker intensity (purple and black curves in Figure 3.6 (a)). In Figure 3.6 (b) we see how even the weakest possible pacemaker with $\psi = 0.06$ attracts the center of the LCG for different initial conditions, but the motion of the center is more pronounced in these curves than in the black curve in panel (a), which corresponds to the full pacemaker.

Next, we study the position of the center $c(t)$ of the LCG throughout 100 independent realizations for each pacemaker in-

tensity. For every time step t and every control intensity ψ, we thus have a distribution $C(c(t), \psi)$ of the position of the LCG center. For the uncontrolled system, there cannot be any preferred position for the LCG of the chimera state over time and across different realizations. The distribution $C(c(t), 0)$, corresponding to the uncontrolled system, is shown in Figure 3.7(a). As we can see from the blue curve in Figure 3.7 (e), the distribution $C(c(t), 0)$ is uniform on $\mathcal{L}$ during the interval W_2. As soon as we break the symmetry of the coupling topology of the network, the distribution of the position of the center changes and we see how the center position is attracted by the partial or full pacemaker. Figure 3.7(b), (c), (d) shows the effect of increasing the pacemaker intensity ψ in position 25. In Figure 3.7 (b) only 2 incoming links of oscillator 25 were cut, while 18 links were removed in panel (c) (corresponding to $\psi = 0.06$ and $\psi = 0.5$, respectively). Figure 3.7 (d) corresponds to 36 links removed, i.e. the full pacemaker ($\psi = 1$). The control effect is clearly visible already in panel (c). Looking at the time averaged spatial distributions in panel (e) one can also observe how these become narrower with a pronounced peak around position 25 as we approach the case of the full pacemaker (see Figure 3.7 (e), black curve).

To further quantify the effects of our control mechanism, we define the following order parameter:

$$\rho(t, \psi) = \left| \frac{1}{2N} \sum_{l \in \mathcal{L}} C(c(t), \psi) e^{i\theta_l} \right|, \tag{3.1}$$

where $\theta_l = \frac{2\pi l}{N}$ for $l \in \mathcal{L}$, t is in the evaluation interval W_2 and $|\cdot|$ is the modulus of complex numbers. We calculate the order parameter $\rho(t, \psi)$ for 20 distributions of the LCG center position which were obtained from 20 sets of 100 independent initial conditions. For every pacemaker intensity ψ we obtained order parameters

$\rho_1(t,\psi),\ldots,\rho_{20}(t,\psi)$, average distances $d_1(t,\psi),\ldots,d_{20}(t,\psi)$ and average LCG sizes $s_1(t,\psi),\ldots,s_{20}(t,\psi)$. We then calculated the mean of their temporal averages over the interval W_2, thus obtaining functions of the pacemaker intensity $\rho(\psi),\ d(\psi),\ s(\psi)$. These values are shown in Figure 3.8 (a),(b),(c). In panel (a) we see how the value of $\rho(\psi)$ sharply increases when passing from pacemaker intensity $\psi = 0$ to $\psi = 0.06$ (the lowest possible intensity in this setting), and then increases more slowly towards the value corresponding to the full pacemaker. The results in Figure 3.8 confirm that the pacemaker attracts the LCG, in the sense that the distance $d(\psi)$ of the LCG center from the pacemaker position decreases as the pacemaker intensity ψ increases. In panel (c) another effect of our control mechanism is shown: an increase in the size $s(\psi)$ of the LCG.

The last step of our analysis is to modify only one value of G. We repeated the analysis described before, setting the value of the coefficient $G(25,7) = \xi$, where $7 = p - R$ and ξ goes from 1 (unchanged matrix G) to 0 (one unidirectional link). Results are represented in Figure 3.8 (d), (e), (f). In panel (d) we observe an increase of the order parameter $\rho(\xi)$ when the modification of the coupling matrix becomes stronger. In particular we see that, as we decrease the value of $G(25,7) = \xi$ (which corresponds to increasing the control intensity), the distribution of the position of the LCG center becomes more and more similar to the one obtained in Figure 3.7 (b), where two links were made unidirectional, as it is reflected in the increasing values of $\rho(\xi)$ (Figure 3.8 (d)) and the decreasing values of the distance $d(\xi)$ of the LCG center from the pacemaker (Figure 3.8 (e)). The effect on the size of the LCG shown in Figure 3.8 (f) is not as pronounced as it was in the case of the transition from no control to the full pacemaker.

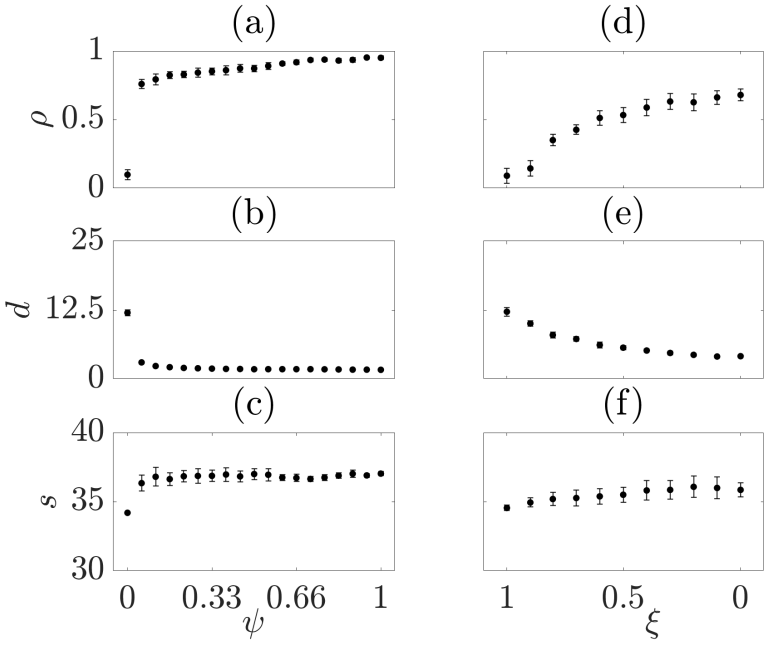

Figure 3.8: Partial pacemaker is sufficient to control the chimera's position. Panel (a) shows the order parameter $\rho(\psi)$. In panel (b) we display values of the distance $d(\psi)$ of the LCG center from the pacemaker position $p = 25$. The average size s of the LCG is shown in panel (c), depending on the pacemaker intensity ψ. Panels (d),(e),(f) are analogous to (a),(b),(c) respectively, but here ρ, d, s are calculated for varying $\xi = G(25, 7)$. For $\xi = 1$ we have the uncontrolled system, while $\xi = 0$ corresponds to one unidirectional link. In all panels, the network size is $N = 50$, the coupling range is $R = 18$ and the phase lag is $\alpha = 1.46$. All time averages were calculated over the evaluation interval W_2. The error bars display the standard deviation of the averages over the 20 sets of 100 independent initial conditions.

3.4 Control Impact

In the previous section we introduced the order parameter ρ to measure the controlling effect of the pacemaker across many realizations. It is also useful to define a quantity that measures how controlled the position of a chimera state is over time. To do this, we define the control impact Γ. We introduced this measure for our studies of multilayer networks of FitzHugh-Nagumo neurons which is the subject of Chapter 5 and our publication [83]. It can however be defined for single layer networks of phase oscillators. We therefore include its definition already here. Following the algorithm in Section 2.2.2, we calculate the position $c(t)$ of the center of the chimera's low coherence group. The center position $c(t)$ takes integer and half-integer values c in the interval $[0.5, N]$. We then define a binary function λ that codifies the evolution of this center position in space and time:

$$\lambda(c,t) = \begin{cases} 1 & \text{if } c = c(t) \\ 0 & \text{otherwise.} \end{cases} \tag{3.2}$$

Denoting the temporal average over the evaluation interval W by $\langle\,\rangle_W$, we define $\gamma(c) = \langle\lambda(c,t)\rangle_W$, which determines the proportion of times for which the center of the low coherence group was in every possible position. We then define the control impact $\Gamma(p,\Delta)$ as

$$\Gamma(p,\Delta) = \sum_{c=p-\Delta}^{p+\Delta} \gamma(c). \tag{3.3}$$

This control impact counts how many times the center of the chimera's low coherence group lies in a neighborhood of width $2\Delta+1$ of the pacemaker position p during the interval W. This corresponds to the area highlighted in green in Figure 3.9(b),(d).

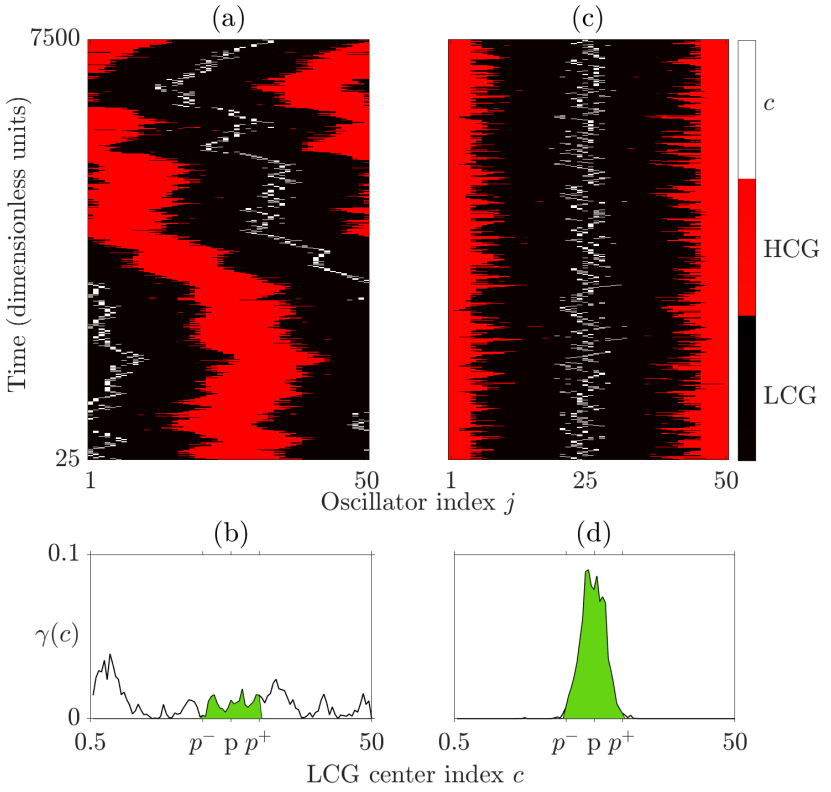

Figure 3.9: Control impact. Different chimera states arise from the same initial conditions in a network of phase oscillators without control (a) and with a pacemaker (c) in position $p = 25$. Panel (b) and (d) show the distribution γ of the position of the LCG center. The green area corresponds to the control impact $\Gamma(25, 5)$ where $p = 25$ and $\Delta = 5$ ($p^{\pm} = p \pm \Delta$). Network parameters: $N = 50$, $R = 18$, $\alpha = 1.46$.

It follows from the definition (3.3) that the control impact takes values between 0 and 1. In an uncontrolled network, there is no preferred position for the center of the low coherence group. Therefore, when the evaluation window W becomes arbitrarily long, the expected value of Γ is $\frac{4\Delta+1}{2N}$. This means that the center of the chimera's low coherence group is equally likely to occupy all positions $c \in [0.5, N]$ while it drifts along the network (Figure 3.9(a), (b)). If the low coherence group is attracted by a pacemaker then $\gamma(c)$ has a pronounced peak around the pacemaker positon and flat tails, therefore Γ has a value close to 1 (Figure 3.9(c), (d)).

3.5 Alternative symmetry breaking mechanism

To further understand which are the important aspects of the control mechanism introduced in this paper, we analyze here what happens when we reverse the pacemaker idea. That is, we select one oscillator with index p and we cut all of its outgoing links. In terms of the coupling matrix G of Eq. (2.1), this corresponds to setting $G(j, p) = 0$ for a fixed column p and for all $j \neq p$. This new configuration is equivalent to isolating oscillator p from the rest of the network, but we continue to show its dynamics in our results. Figure 3.10 shows what happens when we repeat the simulations of Figures 3.1, 3.3, 3.4 substituting the pacemaker with the new symmetry breaking configuration, which consists in cutting the outgoing links of oscillator $p = 18$. Panels (a), (b) and (c) of Figure 3.10 are replicas of panels (a), (b), (c) of Figure 3.1 (uncontrolled chimeras), and we can see how the remaining panels of Figure 3.10 are qualitatively similar to the corresponding panels obtained in Figures 3.3, 3.4 using the full pacemaker. These findings show that the essential element for chimera control is the disruption of the

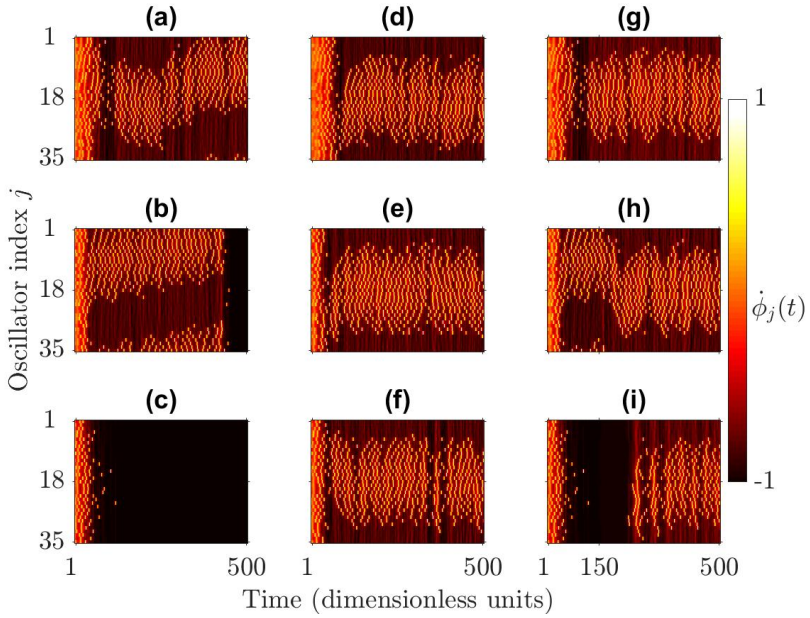

Figure 3.10: Cutting the outgoing links of one oscillator acts like a full pacemaker. In panels (a), (b), (c), we display instantaneous phase velocities for three different realizations of Eq. (2.2) for $N = 35$, $R = 12$, $\alpha = 1.46$, $\omega = 0$ (same initial conditions as in Figures 3.1, 3.3, 3.4). In panels (d), (e), (f) we display the effects of the symmetry breaking described in Section 3.5 with $p = 18$ on the solutions shown in panels (a), (b), (c) respectively. The symmetry breaking was activated at the beginning of the simulations. Panels (g), (h), (i) are analogous to panels (d), (e), (f) but here the symmetry breaking was activated after 150 dimensionless time units.

spatial symmetry of the ring network.

3.6 Discussion

We introduced a method based on the idea of a pacemaker oscillator which allows one to control chimera states in small networks of phase oscillators. By varying the control intensity, we were able to investigate which is the minimal action needed to control chimera states. We found that modifying only one coefficient in the connectivity matrix is enough to control the chimera's position. Appealing features of our method are the simplicity of its implementation, which lies in the fact that no feedback from the system is needed and that it does not intervene on the oscillators' parameters. Interestingly, there are strong analogies between our results and the ones elaborated by Isele and colleagues [38]. Although they use a different model and a completely different control mechanism, they also observed that the symmetry breaking element in the network attracts the low coherence group and stabilizes the chimera state. The effects of symmetry breaking in the evolution of chimera states also emerge in the recent work by Yao et al. in Ref. [106]. They perturbed the dynamics of a ring-shaped network of phase oscillators by selecting a target oscillator and forcing it to have a fixed phase difference with respect to the local mean field of its neighbours. This perturbation induces the low coherence group to be centered around the target oscillator. Our results confirm the occurrence of this self-adaptation [106] of the chimera position, and generalize the findings in Ref. [106] showing that weaker changes in the network are sufficient not only to control the chimera's position, but also to trigger chimeras for parameters and initial conditions for which they do not form spontaneously. Moreover, the full pacemaker can be used to generate a chimera state after the system has collapsed to the synchronous solution.

It is worth to point out that the idea of a pacemaker was already introduced in the study of synchronization of the Kuramoto model. In Ref. [43, 77] a pacemaker was used to synchronize random networks of phase oscillators. We showed that the same mechanism produces the opposite effect for the Kuramoto-Sakaguchi model. In fact, it promotes the existence of chimera states when the oscillators are nonlocally coupled. This comparison underlines the importance of the interplay of nonlocal coupling, the phase lag and the control mechanism in the control of chimera states. Given that our method acts exclusively on the connectivity of the network and not on the intrinsic dynamics of the oscillators, we conjecture that it may work also for networks made of different types of oscillators and more complex topologies. To verify this conjecture will be the scope of the next two chapters.

CHAPTER 4

Control of chimera states in multiplex networks of phase oscillators

As we discussed in Chapter 1, the study of chimera states in multilayer networks represents a growing field of research [5, 7, 20, 27, 32, 54, 55, 57, 59, 86, 87, 89, 104]. In this chapter we briefly review previous work about synchronization of chimera states across the different layers of a multilayer network and then we generalize the control mechanism introduced in Chapter 3 to multiplex networks of phase oscillators. We want to answer three main questions: is it possible to remotely control a chimera states in layer 2 via the coupling, using a pacemaker in layer 1? Is a pacemaker stronger than interlayer coupling or viceversa? And finally, which is the effect of having pacemakers in both layers, but in antipodal positions?

4.1 Synchronization between chimera states

When considering multilayer networks it is important to assess the synchronization of the dynamics in the different layers. In 2017, Andrzejak and coauthors found that chimera states in a multiplex network can enter in a regime of generalized synchronization [5]. For nonidentical systems it is impossible to synchronize identically, but there can be a relationship between the dynamics due to the coupling. If we consider two systems X, Y with a driver-response coupling from X to Y, then we say that there is generalized synchronization between X and Y if there exists a function F such that $Y = F(X)$ [81]. This means that the dynamics of Y is completely determined by the dynamics of X, although in general the function F may be arbitrarily complex and difficult to detect. In Ref. [5] the authors used the auxiliary system approach to detect generalized synchronization [1]. In this approach one considers an identical copy Y' of the repsonse system Y which is also driven by X. If Y and Y' get identically synchronized after being initialized with different initial conditions, then there is generalized synchronization between X and Y. This is because, if there is generalized synchronization, the states of Y and Y' are completely determined by X and not by their respective initial conditions. The concept of generalized synchronization has some limitations which make it difficult to apply in realistic systems. First, generalized synchronization is only defined for a driver-response configuration. In the context of chimera states, this implies that we can only use this concept in multiplex networks with unidirectional coupling. Secondly, methods to detect the existence of the function F such that $Y = F(X)$ can be difficult to apply in realistic scenarios. For example, it may not be possible to construct an identical copy of Y driven by X.

To further invesitgate how chimeras can synchronize, in Ref.

[7] the authors extended the previous study [5] to more realistic settings and proposed to use the concept of phase synchronization introduced for low dimensional chaotic systems [80] to study chimeras in multilayer networks with layers of different sizes and bidirectional coupling between them. The coupling between the layers was obtained using the mean-field obtained from the phase of the order parameter (Eq. (2.5)). For sufficiently strong coupling, the phases of the order parameters of the two layers became weakly locked [7].

In this thesis we study a weaker kind of synchronization linked to the position of the chimera states within the layers. In Ref. [5] the authors already observed how, along with generalized synchronization, the chimeras in different layers align their positions. Here we further investigate this effect and see whether it can be enhanced or suppressed using the pacemaker control.

4.2 Model and integration

We consider a multiplex network with two layers of N phase oscillators each [5]. Each layer is a ring network of nonlocally coupled phase oscillators with a rectangular kernel of broadness R (see Section 2.2, Eq. (2.2)). Each variable $\phi_{1j}(t)$ in layer 1 is coupled to the corresponding phase $\phi_{2j}(t)$ in layer 2, with $j = 1, \ldots, N$ [5]:

$$\begin{aligned}
\dot{\phi}_{1j}(t) &= \omega - \frac{1}{2R}\sum_{k=j-R}^{j+R} \sin(\phi_{1j}(t) - \phi_{1k}(t) + \alpha_1) \\
&\quad - \sigma_{2\to1} \sin(\phi_{1j}(t) - \phi_{2j}(t)) \\
\dot{\phi}_{2j}(t) &= \omega - \frac{1}{2R}\sum_{k=j-R}^{j+R} \sin(\phi_{2j}(t) - \phi_{2k}(t) + \alpha_2) \\
&\quad - \sigma_{1\to2} \sin(\phi_{2j}(t) - \phi_{1j}(t)).
\end{aligned} \tag{4.1}$$

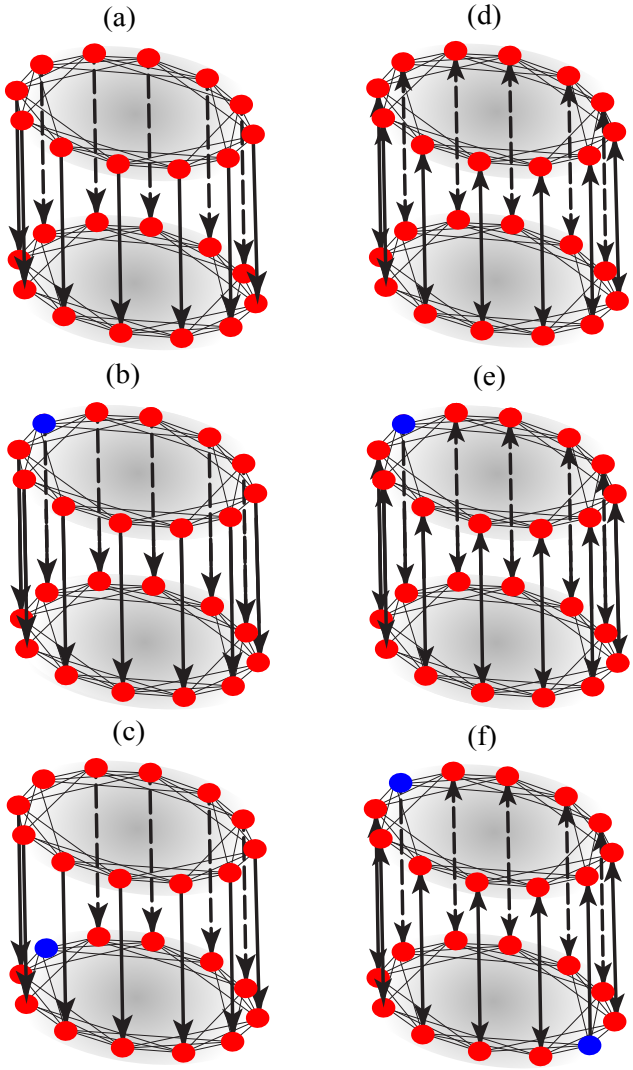

Figure 4.1: Different combinations of multiplexing and control. Multiplex networks formed by two layers with nonlocal coupling. Red circles are the oscillators and the blues ones are the oscillators which act as pacemaker. The left column corresponds to unidirectional coupling. (a) No control, (b) pacemaker in layer 1, (c) pacemaker in layer 2. The right column corresponds to bidirectional coupling between the layers. (d) No control, (e) pacemaker in layer 1, (f) pacemakers in layer 1 and layer 2 in antipodal positions.

If $\sigma_{1\to 2} > 0$ and $\sigma_{2\to 1}$ is zero, then we have unidirectional coupling, corresponding to a driver-response configuration. If also $\sigma_{2_\to 1} > 0$, then we set $\sigma_{2\to 1} = \sigma_{1\to 2} = \sigma_{1\leftrightarrow 2}$ and we obtain a bidirectional coupling scheme. We introduce a mismatch between the layers via the phase-lag parameters α_2 as we set $\alpha_2 = \alpha_1 + \Delta\alpha$ [5].

All equations are integrated using the classical fourth-order Runge-Kutta algorithm with time step $dt = 0.01$ spanning 10^6 time steps, corresponding to 10^4 dimensionless time units. We caculate averages in a time window W of 2500 dimensionless units positioned at the end of the simulation.

Since in this chapter we are focusing on controlling the position of chimera states, each time we start the system with random initial conditions, we use the order parameter defined in Eq. (2.5) to check whether the system has synchronized and, if this is the case, we discard the realization and restart the simulation, following the strategy described in Ref. [5].

We use a pacemaker oscillator [82] to control chimera states in one or both layers. The details on how to implement this control mechanism were explained in Chapter 3, section 3.2. There are many possibilities regarding the position of the pacemaker or pacemakers within the multiplex structure. Here, we will first consider the situation in which no control is present and then four different configurations in which 1 or 2 pacemakers are present. In Figure 4.1 we show schematic representations of the six configurations that we will consider in this chapter. The first row corresponds to unidirectional coupling between the layers (Fig. 4.1(a), (b), (c)) and the second one to bidirectional coupling (Fig. 4.1(d), (e), (f)). The pacemaker oscillators are coloured in blue.

4.3 Control impact and Synchronization

To assess the interplay between chimera states across the two layers we here introduce two quantities that measure the alignment of the low coherence groups of the chimera states and the across-layer synchronization of the two dynamics. First, we want to measure the degree to which the chimera states in the two layers align their positions. To do this we calculate the difference between the positions of the centers of the low coherence groups $c_1(t), c_2(t)$ in the two layers on a ring with circumference of length N:

$$D_{12} = \langle \min\{|c_1(t) - c_2(t)|\,, N - |c_1(t) - c_2(t)|\}\rangle_W\,, \qquad (4.2)$$

where $\langle\,\rangle_W$ continues to denote the time average over the evaluation interval W. To quantify synchronization between the two layers we use a normalized phase difference which was defined in Ref. [5] as follows:

$$\delta_{12}(t) = \frac{1}{N}\sum_{j=1}^{N}\left|\sin\left(\frac{\phi_{2j}(t) - \phi_{1j}(t)}{2}\right)\right| \qquad (4.3)$$

Also for $\delta_{12}(t)$ we calculate the temporal average over the time window W, obtaining $\delta_{12} = \langle\delta_{12}(t)\rangle_W$.

4.4 Results

4.4.1 Unidirectional coupling

We start by studying the position of chimera states and the alignment between their low coherence groups in a multiplex network with two layers organised in a driver-response configuration. This setup is described by Eq. (4.1) with $\sigma_{2\to1} = 0$ and $\sigma_{1\to2} > 0$.

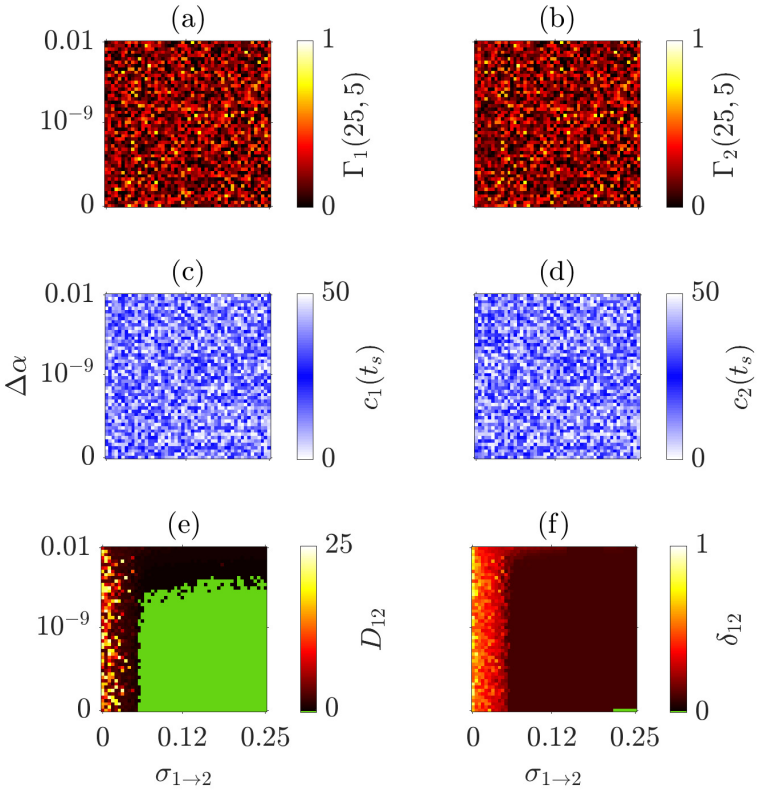

Figure 4.2: Chimera states align across different layers with unidirectional coupling in the absence of control. Results for a multiplex network with two layers of nonlocally coupled phase oscillators. (a), (b) control impact $\Gamma_1(25,5)$ and $\Gamma_2(25,5)$. (c), (d) Snapshots of the position of the LCG centers $c_1(t_s))$ and $c_2(t_s)$ at time $t_s = 500000$ time steps. (e) D_{12}, measure of the alignment between the centers $c_1(t)$ and $c_2(t)$. (f) Normalized phase difference δ_{12}. Network parameters: $N = 50$, $R = 18$, $\alpha_1 = 1.46$.

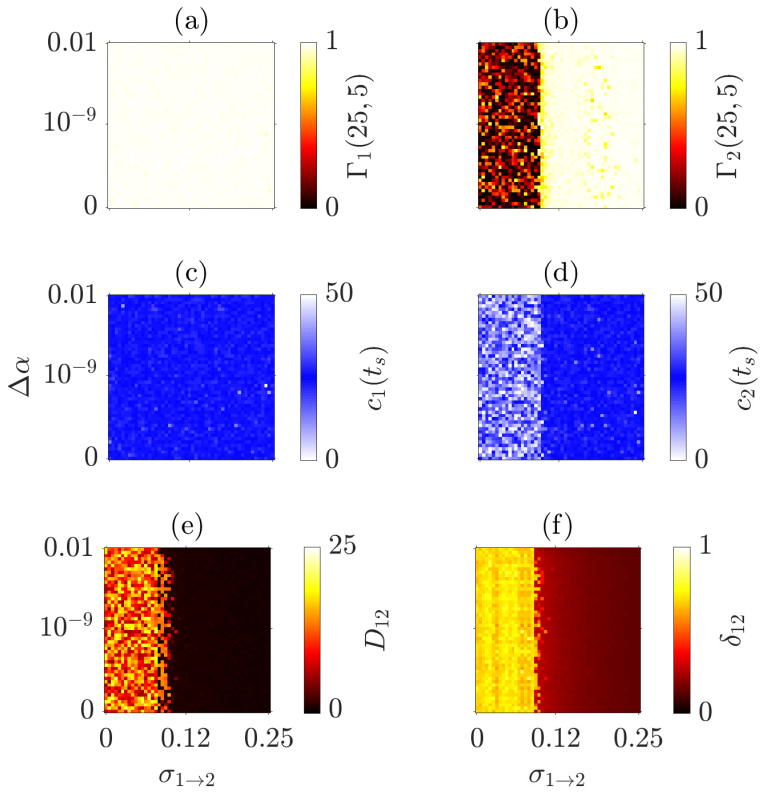

Figure 4.3: A pacemaker in layer 1 can control chimeras in layer 2 through unidirectional coupling. Same as Figure 4.2, but here there is a pacemaker in layer 1, position $p_1 = 25$.

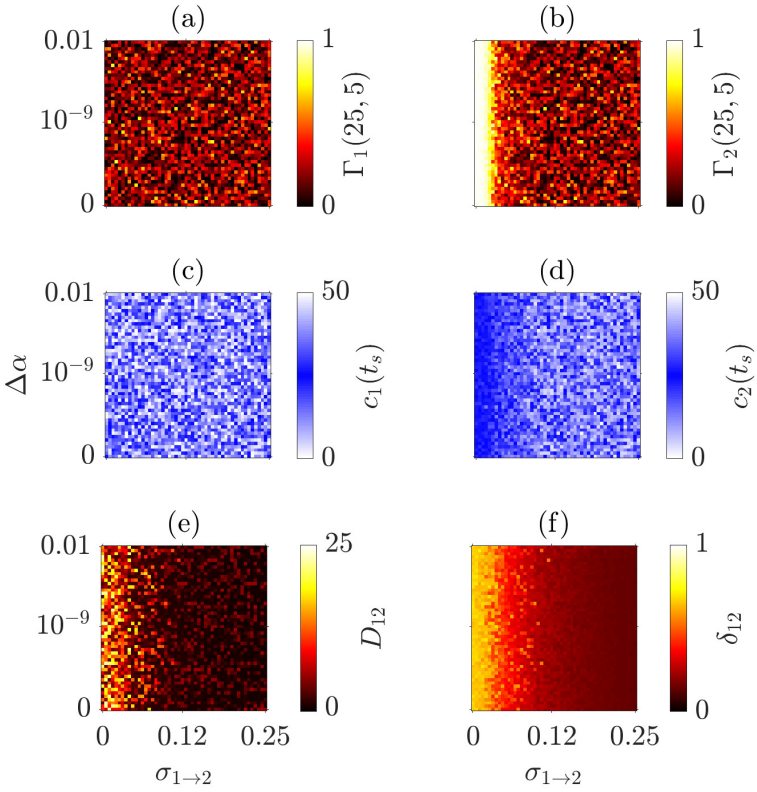

Figure 4.4: The unidirectional coupling is stronger than a pacemaker. Same as Figure 4.2, but here there is a pacemaker in layer 2, position $p_2 = 25$.

The parameter space is spanned by the mismatch $\Delta\alpha$ between the phase-lag parameters α_1 and α_2, and by the interlayer coupling $\sigma_{1\to2}$. The phase-lag mismatch $\Delta\alpha$ is sampled logarithmically in 49 steps from 10^{-15} to 0.01, and we also consider the case of identical systems with $\Delta\alpha = 0$. The interlayer coupling $\sigma_{1\to2}$ is sampled linearly in 50 steps from 0 (which corresponds to isolated layers) to 0.25. Since we plan to have a pacemaker in positon $p = 25$ in layer 1 or layer 2, for each configuration displayed in Figure 4.1(a), (b), (c) and for every pair of $\Delta\alpha$ and $\sigma_{1\to2}$ we calculate the control impact values $\Gamma_1(25, 5)$ and $\Gamma_2(25, 5)$ (for details, see Section 3.4). We also take a snapshot of the position of the centers $c_1(t_s)$, $c_2(t_s)$ at time t_s. We then calculate D_{12} and δ_{12} as defined in Section 4.3. The snapshot time t_s was chosen prior to the averaging window W so that the values $c_1(t_s)$ and $c_2(t_s)$ give us further information on where the center of the low coherence group is found earlier in the simulations.

We start with an uncontrolled network with unidirectional coupling. A schematic view of this configuration is displayed in Figure 4.1(a). This is the same model studied in Ref. [5]. Since there is no preferred position for the low coherence group of the chimera states in uncontrolled networks, we expect a uniform distribution for the values of Γ_1. This is what we see in Figure 4.2(a), where we show values of $\Gamma_1(25, 5)$. This result is also reflected in Figure 4.2(c), where we see a snapshot of the position of the LCG center $c_1(t_s)$. The analogous quantities $\Gamma_2(25, 5)$ and $c_2(t_s)$ for layer 2 behave in a similar fashion (Figure 4.2(b), (d)). In panel (e) we show the distance D_{12} (Eq. 4.2) between the centers of the LCGs $c_1(t)$ and $c_2(t)$ and we can see how the centers are aligned for a wide range of parameters where $D_{12} = 0$. The same holds for the position of the center $c_2(t)$, which is shown in Figure 4.2(d). The interlayer error δ_{12} reaches the value zero only when the two layers are identical, i.e. for $\Delta\alpha = 0$.

As a second scenario, we introduce a pacemaker in layer 1, position $p_1 = 25$ (Figure 4.1(b)). In this case we want to see whether the control can be transferred from layer 1 to layer 2 via the interlayer coupling. In Figure 4.3(a) we see how the position of the low coherence group in layer 1 is controlled by the pacemaker. The control effect exerted by the pacemaker in layer 1 is effective also in layer 2 starting from a value of $\sigma_{1\to2}$ as low as 0.12 as we can see in Figure 4.3(b). This result is reflected in the values of $c_1(t_s)$ and $c_2(t_s)$ (Figure 4.3(c) and (d) respectively). As a consequence, the centers become aligned for increasing coupling (Figure 4.3(e)). In this case δ_{12} never becomes zero because the presence of the pacemaker makes the two layers non-identical even for $\Delta\alpha = 0$.

Finally, we study what happens when we introduce a pacemaker only in layer 2, in position $p_2 = 25$. Given that layer 2 is driven by layer 1, we use this configuration to answer the second of the three questions that we asked at the beginning of this chapter, whether a pacemaker can overrule the driving. Since layer 1 does not receive any input from layer 2, the behaviour of the LCG center is the same as in the first case considered in this section, so we see that the coupling impact $\Gamma_1(25, 5)$ in Figure 4.4(a) looks similar to Figure 4.2(a). In layer 2, the pacemaker attracts the center of the low coherence group around its position $p_2 = 25$ for low coupling $\sigma_{1\to2}$ which causes the control impact $\Gamma_2(25, 5)$ to take values close to 1 (white area in Figure 4.4(b)). As the coupling increases though, we see how the pacemaker cannot control the position of the center anymore, and Γ_2 follows the pattern of Γ_1. This behaviour is reflected in the distributions of the values of $c_1(t_s)$ and $c_2(t_s)$ in Figure 4.4(c) and (d), respectively. Since now there is a pacemaker in layer 2, identical synchronization is not achieved even for $\Delta\alpha = 0$. We see in Figure 4.4(e) that the centers of the low coherence groups never completely align. Also the normalized phase difference δ_{12} takes always positive values which get closer

to zero as the coupling increases.

4.4.2 Bidirectional coupling

We now activate also the coupling $\sigma_{2\to1}$ from layer 2 to layer 1, thus obtaining bidirectional coupling between the layers. This configuration corresponds to the schemes in Figure 4.1(d), (e), (f). First we consider what happens if there is no control (Figure 4.1(d)), secondly if there is a pacemaker in layer 1, position $p_1 = 25$ (Figure 4.1(e)) and lastly if there are two pacemakers in the network, in layer 1, position $p_1 = 25$ and in layer 2, position $p_2 = 50$ (Figure 4.1(f)). We compute the same measures $\Gamma_1(25, 5)$, $\Gamma_2(25, 5)$, $c_1(t_s)$, $c_2(t_s)$, D_{12} and δ_{12} as in the previous Section 4.4.1. In the last setting with two pacemakers, $\Gamma_2(25, 5)$ is substituted by $\Gamma_2(50, 5)$.

Following the analysis of the unidirectional case, we start by considering the multiplex network without control (Figure 4.1(d)). The results are shown in Figure 4.5 and they are analogous to the results obtained for unidirectional coupling shown in Figure 4.2. We see that there is no preferred position for the centers of the low coherence groups and that the chimera states quickly align for increasing interlayer coupling (Figure 4.5(a), (b), (c), (d)). The alignment region in Figure 4.5(e) is comparable to the unidirectional case. The identical synchronization when $\Delta\alpha = 0$ (green line in Figure 4.5(f)) starts from lower values of the interlayer coupling $\sigma_{1\to2}$ compared with the unidirectional case.

When we introduce a pacemaker in layer 1, as in Figure 4.1(e) we observe an interesting effect. The center $c_1(t)$ is attracted by the pacemaker in position $p_1 = 25$ except for a narrow region of parameter space (Figure 4.6(a)). The LCG of the chimera in layer 2 is remotely controlled by the pacemaker in layer 1, as the values of $\Gamma_2(25, 5)$ are close to 1 when the coupling $\sigma_{1\leftrightarrow2}$ becomes stronger. These results are confirmed in Figure 4.6(c), (d) which

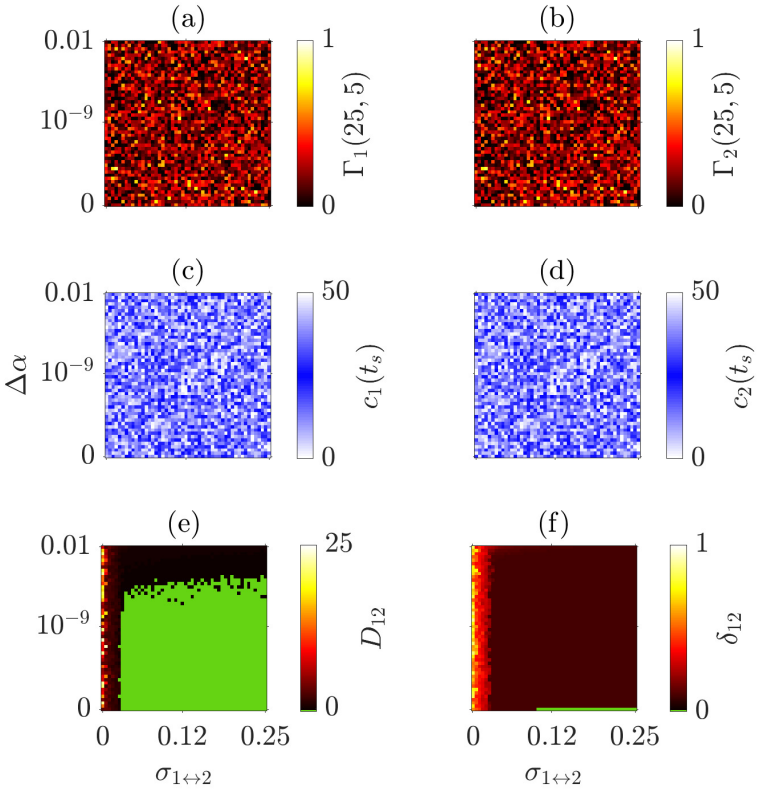

Figure 4.5: Chimera states align across different layers with bidirectional coupling. All parameters are the same as in Figure 4.2, but here there is bidirectional interlayer coupling $\sigma_{1\leftrightarrow 2}$.

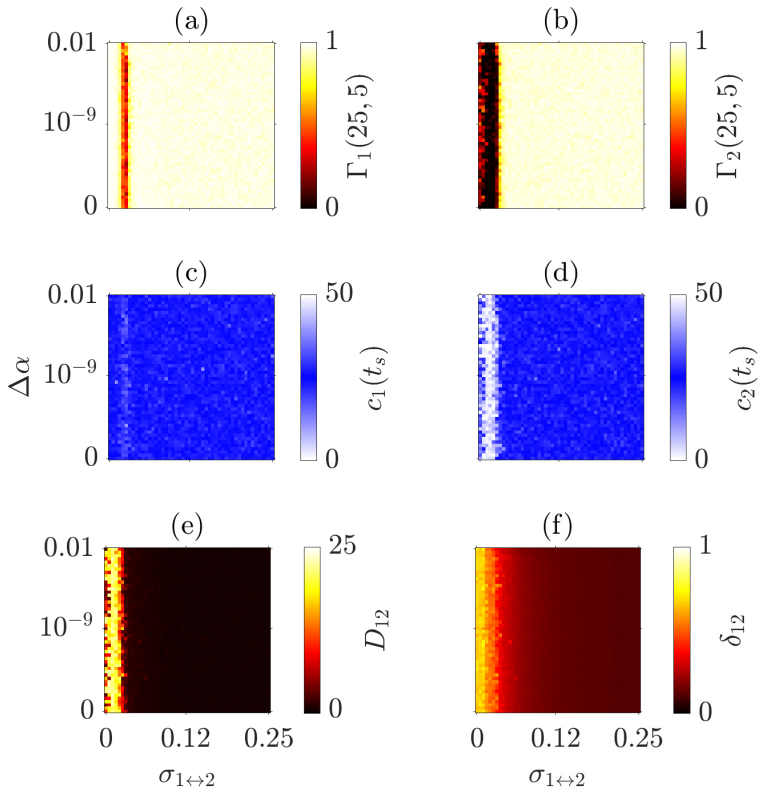

Figure 4.6: A pacemaker remotely controls chimera states through bidirectional coupling. Same as in Figure 4.5, but here there is a pacemaker in layer 1, position $p_1 = 25$.

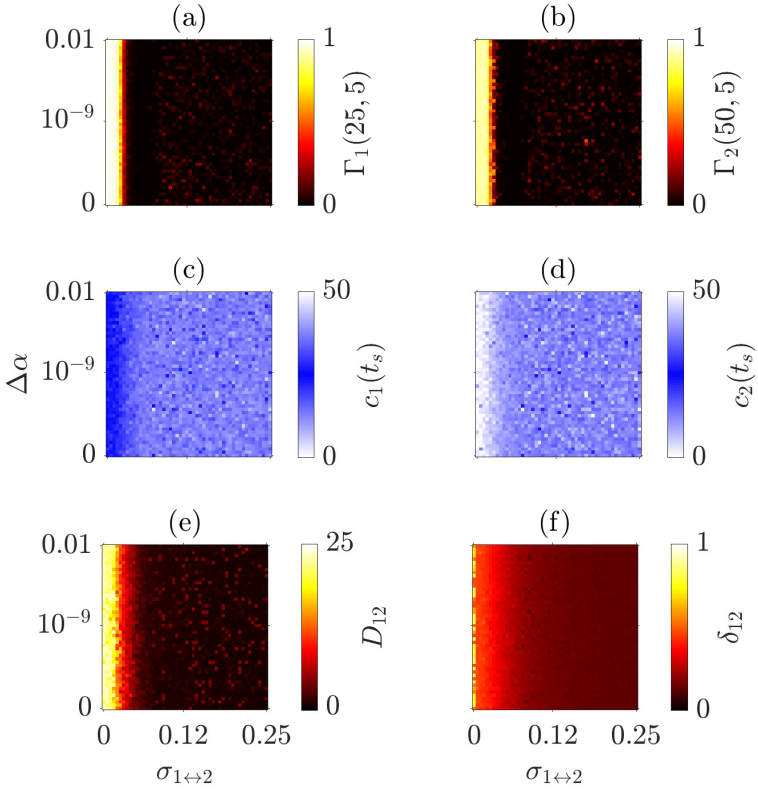

Figure 4.7: Conflicting pacemakers lead chimeras to compromise on a middle position. Same as in Figure 4.5, but here there are two pacemakers: one in layer 1, position $p_1 = 25$ and one in layer 2, position $p_2 = 50$.

show snapshots of the LCG centers c_1, c_2. It follows that the centers are aligned, but in this case we only get values of D_{12} which are low, but still positive. The same holds for the interlayer error δ_{12}, given that now, because of the pacemaker, the two layers are not identical even when $\Delta\alpha = 0$.

Lastly, we investigate what is the effect of having pacemakers in both layers in antipodal positions. We insert a pacemaker in layer 1, position $p_1 = 25$ and one in layer 2, position $p_2 = 50$ (Figure 4.1 (f)). For low coupling $\sigma_{1\leftrightarrow 2}$ both pacemakers are attracting the LCGs to their respective positions. However, as the coupling increases, the values of $\Gamma_1(25, 5)$ and $\Gamma_2(50, 5)$ get close to zero. Looking at the snapshots of the LGC centers c_1 and c_2 in Figure 4.7(c), (d) we understand that this happens because the centers c_1 and c_2 align close to positions that are equidistant from the two pacemakers on the circle (these positions are 12.5 and 37.5).

4.5 Discussion

In this section we demonstrated that a pacemaker can be used to control chimera states in a multiplex network of phase oscillators. Given that the model is more complex with respect to the ring network in Chapter 3, we had to consider a variety of ways in which the pacemaker control can be applied. Our main results are that it is possible to remotely control a chimera state in layer 2 through a pacemaker in layer 1 and that the driving effect is stronger than a pacemaker. The possibility of using remote control is important for situations in which one has access only to parts of a system. The results obtained for bidirectional coupling strengthen the flexibility of our method, which still shows its effects in a situation in which the layers are mutually influencing each other. Our next challenge now is to investigate whether the pacemaker control works not only with more complex network topologies, but

also with more realistic oscillators. For this purpose, in the next chapter we will generalize the analysis of this chapter to networks of FitzHugh-Nagumo neuron models.

CHAPTER 5

Control of chimera states in networks of FitzHugh-Nagumo oscillators

As a further application of our control method, we use it in multiplex networks of FitzHugh-Nagumo oscillators. This chapter will therefore offer an insight on the possibility of using the pacemaker control with complex node dynamics. We investigate the same multilayer network architectures which we studied in Chapter 4 for phase oscillators, but here for FitzHugh-Nagumo oscillators.

5.1 Model and integration

We study the dynamics of a two-layer network of FitzHugh-Nagumo oscillators. Each unit is characterized by two variables $u(t)$ and $v(t)$. Each layer is formed by N oscillators arranged in a ring topology. Following Ref. [69], inside each layer $l = 1, 2$, the oscillators are coupled nonlocally with range R and strength σ_l (see Section

2.3). The dynamics of the multiplex network is governed by the following set of differential equations [59]:

$$
\begin{aligned}
\epsilon\frac{du_{1j}(t)}{dt} &= u_{1j}(t) - \frac{u_{1j}(t)^3}{3} - v_{1j}(t) \\
&\quad + \frac{\sigma_1}{2R_1}\sum_{k=1}^{N} G_1(j,k)[(b_{uu}(u_{1k}(t) - u_{1j}(t)) + b_{uv}(v_{1k}(t) - v_{1j}(t)))] \\
&\quad + \sigma_{2\to1}(u_{2j}(t) - u_{1j}(t)) \\
\frac{dv_{1j}(t)}{dt} &= u_{1j}(t) + a \\
&\quad + \frac{\sigma_1}{2R_1}\sum_{j=1}^{N} G_1(j,k)[(b_{vu}(u_{1k}(t) - u_{1j}(t)) + b_{vv}(v_{1k}(t) - v_{1k}(t)))] \\
\epsilon\frac{du_{2j}(t)}{dt} &= u_{2j}(t) - \frac{u_{2j}(t)^3}{3} - v_{2j}(t) \\
&\quad + \frac{\sigma_2}{2R_2}\sum_{k=1}^{N} G_2(j,k)[(b_{uu}(u_{2k}(t) - u_{2j}(t)) + b_{uv}(v_{2k}(t) - v_{2j}(t)))] \\
&\quad + \sigma_{1\to2}(u_{1j}(t) - u_{2j}(t)) \\
\frac{dv_{2j}(t)}{dt} &= u_{2j}(t) + a \\
&\quad + \frac{\sigma_2}{2R_2}\sum_{k=1}^{N} G_2(j,k)[(b_{vu}(u_{2k}(t) - u_{2j}(t)) + b_{vv}(v_{2k}(t) - v_{2j}(t)))].
\end{aligned}
\tag{5.1}
$$

Regarding the interlayer coupling scheme, Eq. (5.1) models a bidirectional multiplex configuration where each oscillator's $u_{1j}(t)$ variable in layer 1 is coupled to the corresponding $u_{2j}(t)$ variable in layer 2, and viceversa. The interlayer coupling strength is $\sigma_{2\to1}$ from layer 2 to layer 1, and $\sigma_{1\to2}$ in the other direction. We also consider unidirectional coupling, i.e. a driver-response configuration which corresponds to $\sigma_{1\to2} > 0$ and $\sigma_{2\to1} = 0$.

We integrated the system using a fourth order Runge-Kutta algorithm with a time-step of 0.01 and we took an integration interval of 10^6 time steps. We then excluded transients from the measurements by taking an evaluation interval W in which the first 10^4 steps are discarded. Following [69], for each layer, initial conditions were taken to be uniformly distributed on a circle of radius 2.

As control mechanism we use a pacemaker oscillator in one or both layers. We implement the control and interlayer coupling like we did in Chapter 4 for multiplex networks of phase oscillators. The different configurations are the ones illustrated in Figure 4.1.

5.2 Control impact and synchronization

In Eq. (2.14) we described how to extract phases $\phi_j(t)$ from the variables $u_j(t), v_j(t)$ of the FitzHugh-Nagumo oscillators. Once we calculate these phases, we can use the measures introduced in the previous chapters for phase oscillators. To study the interplay of control and interlayer coupling in multiplex networks of FitzHugh-Nagumo oscillators we use the control impact Γ introduced in Section 3.4 (see Figure 3.9). To assess the degree of alignment of the two chimera states, we use the distance D_{12} defined in Eq. (4.2) which measures the distance between the centers of the incoherent groups $c_1(t), c_2(t)$. The centers are calculated applying the algortihm in Section 2.2.2 to the phases $\phi_j(t)$. To study the synchronization between the dynamics of the two layers we use the measures introduced in Ref. [87]. For $j = 1, \ldots, N$, the local interlayer synchronization error is defined as:

$$E_{12}(j) = \langle \| x_{1j}(t) - x_{2j}(t) \| \rangle_W \,, \tag{5.2}$$

where $x_{lj} = \begin{bmatrix} u_{lj} \\ v_{lj} \end{bmatrix}$ for $l = 1, 2$, and $\| \ \|$ is the euclidean norm. By taking also the spatial average in Eq. (5.2), one obtains the global interlayer synchronization error [87]:

$$E_{12} = \frac{1}{N} \sum_{j=1}^{N} E_{12}(j). \tag{5.3}$$

5.3 Results

5.3.1 Unidirectional coupling

First we consider the case of unidirectional interlayer coupling from layer 1 to layer 2. We study three possible configurations: without any control, with a pacemaker in layer 1 in position $p_1 = 25$ and finally with a pacemaker in layer 2 in position $p_2 = 25$ while layer 1 is uncontrolled.

Figure 5.1(a), (b) confirms that in the absence of a control mechanism there cannot be any preferred position for the center of the incoherent group. This is reflected in values of $\Gamma_1(25, 5)$ and $\Gamma_2(25, 5)$ that are close to the expected value of $\frac{4\Delta+1}{2N}$. This means that in each realization the drifting causes the chimera's center to occupy all positions almost uniformly. This is confirmed by the snapshot of the centers of incoherence shown in Figure 5.1(c), (d). At a certain moment in time, the center of the LCG is in different positions in different realizations. For strong interlayer coupling, the incoherent groups of the chimera states align (dark area in Figure 5.1(e)) and, in general, the two layers synchronize their dynamics, as it is shown in Figure 5.1(f) where the global synchronization error E_{12} reaches values close to zero.

The scenario described so far in the uncontrolled case is quite intuitive, while it is less obvious what happens when there is also

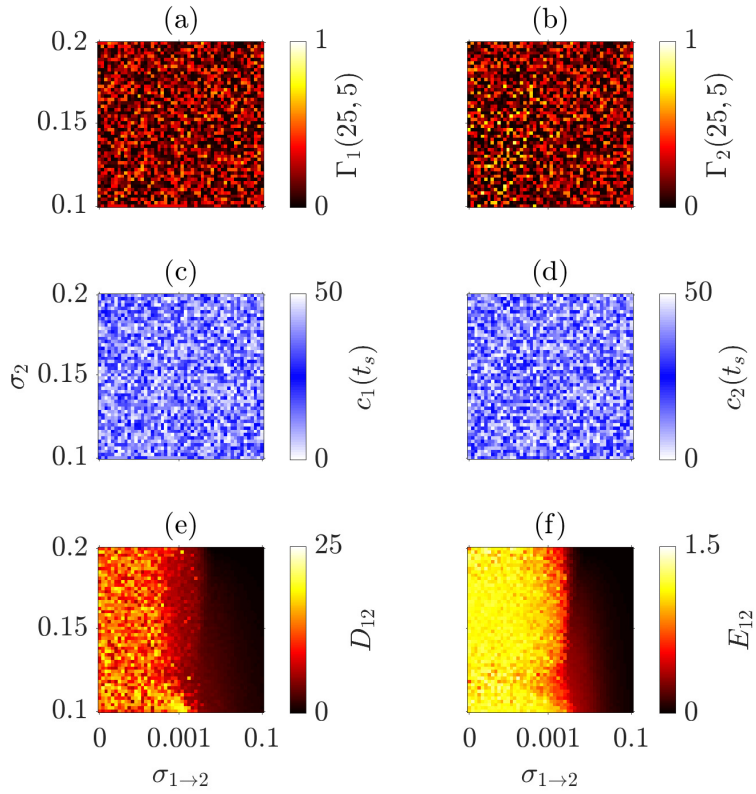

Figure 5.1: Unidirectional coupling causes alignment of chimera states in a two-layer network of FitzHugh-Nagumo oscillators. The interlayer coupling $\sigma_{1\to2}$ varies from 0 to 0.05 and the nonzero values are sampled on a logarithmic scale, while $\sigma_{2\to1}$ is kept equal to 0. The intralayer coupling σ_2 varies linearly from 0.1 to 0.2. Other parameters are: $N = 50$, $R = 18$, $\sigma_1 = 0.2$, $\phi = \pi/2 - 0.1$. Panels (a) and (b) show control impact values $\Gamma_1(25, 5)$ and $\Gamma_2(25, 5)$, while panels (c) and (d) are snapshots of the position $c_l(t_s)$ of the LCG center with $t_s = 500000$ in layer $l = 1, 2$, respectively. The rightmost column shows synchronization measures: the alignment D_{12} in panel (e) and the global synchronization error E_{12} in panel (f).

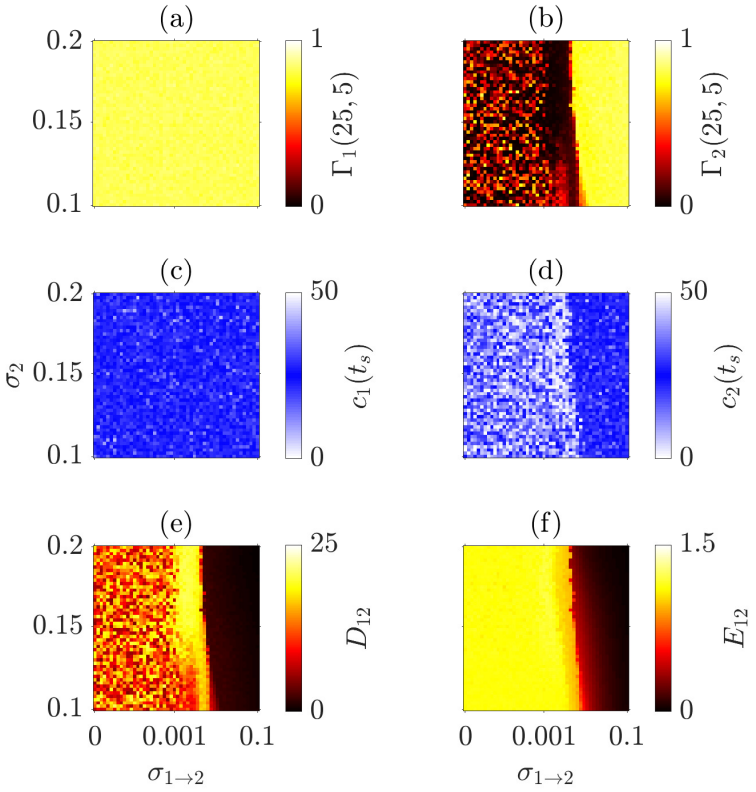

Figure 5.2: Unidirectional coupling, pacemaker in layer 1: remote control of one layer through a pacemaker in the other. Same as Figure 5.1, but here there is a pacemaker in layer 1 in position $p_1 = 25$.

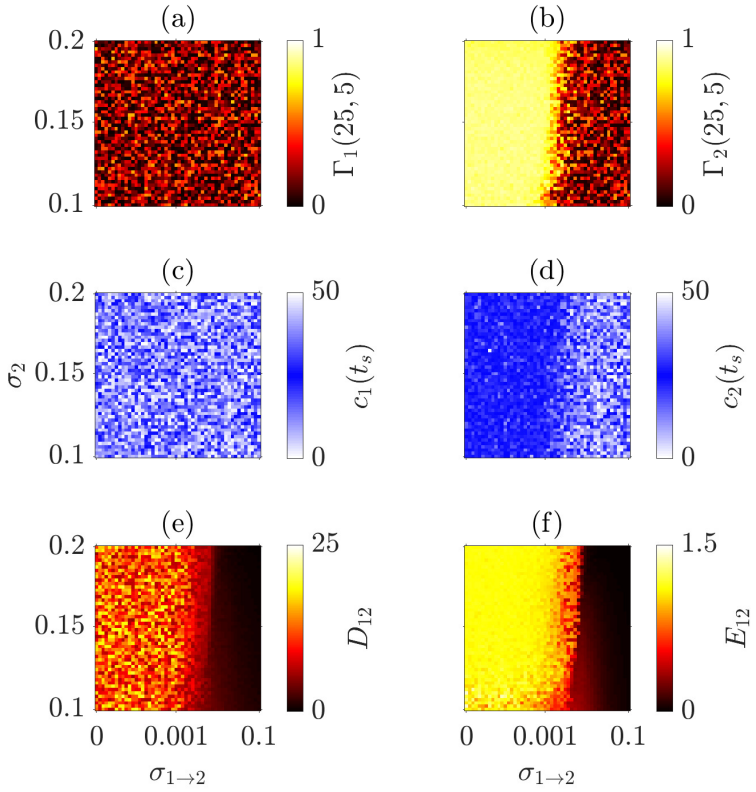

Figure 5.3: Unidirectional coupling, pacemaker in layer 2: the driving becomes stronger than control. Same as Figure 5.1, but here there is a pacemaker only in layer 2 in position $p_2 = 25$.

a pacemaker present in the network. The results for the second configuration, obtained for a network with a pacemaker in position $p_1 = 25$ of the driving layer (layer 1), are shown in Figure 5.2. Because of the unidirectional coupling, layer 1 is not receiving any input from layer 2, therefore it behaves as an isolated ring network. The almost constant value of $\Gamma_1(25, 5)$ close to 1 shows that the pacemaker can control the position of a chimera state (Figure 5.2(a)) in an isolated layer of FitzHugh-Nagumo oscillators. These new results generalize our observations for phase oscillators in Chapter 4 to FitzHugh-Nagumo oscillators. The question now is whether the pacemaker in layer 1 can remotely control the position of the chimera state in layer 2 via the coupling. When the chimeras are aligned across the layers (see Figure 5.2(e) and (f)), we see that the answer is affirmative (yellow region in Figure 5.2(b)). It is worth noticing that before the control becomes effective in layer 2 there is an intermediate region of parameters in which we observe that the center of the incoherent group in layer 2 tends to be diametrically opposed to the pacemaker position (yellow region in Figure 5.2(e)). This means that the distance between the centers of the two low coherence groups reaches its maximum. The pacemaker has a repulsive action on the center of incoherence in layer 2 before the remote control starts to be effective.

Another interesting question is which one is stronger, the pacemaker or the driving? To address this problem, we move to the third configuration. In this case we still have unidirectional coupling from layer 1 to layer 2 and a pacemaker only in position $p_2 = 25$ of layer 2. As a consequence, there is no preferred position for the chimera states in layer 1, as we can see from the values of $\Gamma_1(25, 5)$ in Figure 5.3(a). In fact, Figure 5.3(a) is equivalent to Figure 5.1(a) (uncontrolled case). As the chimera states align for high values of the interlayer coupling $\sigma_{1\to2}$ (Figure 5.3(b) and (e)), the driving effect of layer 1 eventually wins over the controlling effect of the

pacemaker in layer 2 (Figure 5.3(b)). Nevertheless, it is interesting that there is a wide region in the parameter space in which it is possible to control the position of the chimera in layer 2 despite the driving by layer 1.

5.3.2 Bidirectional coupling

We now consider bidirectional interlayer coupling and three possible configurations: without any control, with a pacemaker in layer 1 in position $p_1 = 25$ and lastly with two conflicting pacemakers, one in layer 1 in position $p_1 = 25$ and one in layer 2 in position $p_2 = 50$. We vary the parameter σ_2 like in the unidirectional case and the parameter $\sigma_{1\leftrightarrow 2}$ like $\sigma_{1\to 2}$ in the unidirectional case.

In the first configuration (Figure 5.4), we observe a similarity with the results obtained in the case of unidirectional coupling (Figure 5.1). In this case, again there cannot be any preferred position for the chimera states in the two layers (Figure 5.4(a) and (b)). This is reflected also in the snapshots of the center positions $c_1(t_s), c_2(t_s)$ in Figure 5.4(c) and (d). The incoherent groups become aligned through a monotonic process (Figure 5.4(e)) and in the same way the dynamics of the two layers become synchronized for increasing interlayer coupling (Figure 5.4(f)).

The second configuration, in which a pacemaker is present in layer 1 at position $p_1 = 25$, leads to results that are different from the unidirectional case. In Figure 5.5(a) we see that the pacemaker is able to control the chimera's position in layer 1 only up to a certain value of interlayer coupling $\sigma_{1\leftrightarrow 2}$ (yellow region). Above this value, the coupling between the layers takes over and the chimera states are aligned (Figure 5.5(e)), but still do not have a preferred position. The main difference with the unidirectional case is that the remote control of the chimera state in layer 2 via the pacemaker in layer 1 and the coupling is possible only in a small

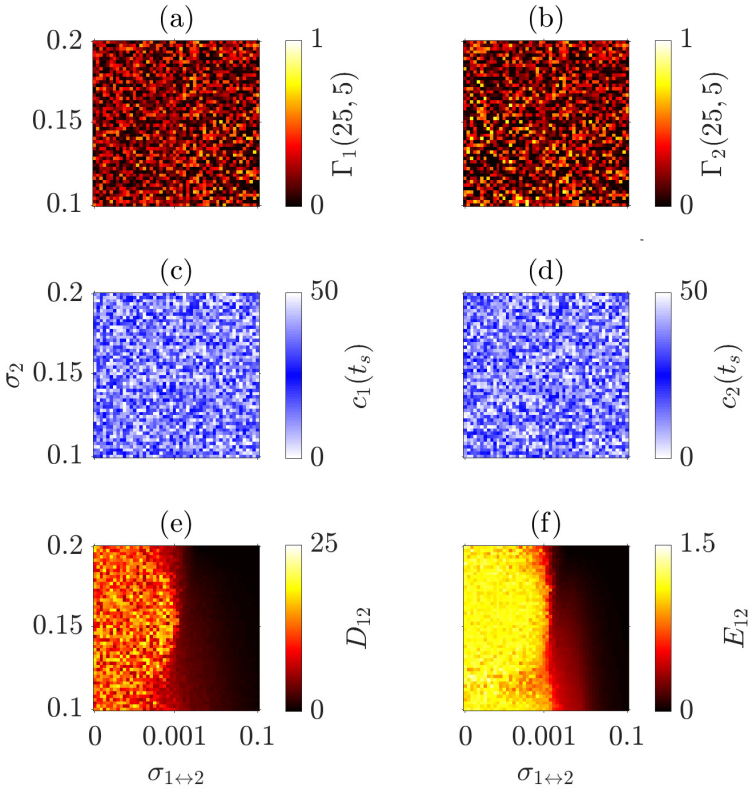

Figure 5.4: Bidirectional coupling favours the alignment of chimera states across layers in the absence of control. Same as Figure 5.1. Here we have $\sigma_{2\to 1} = \sigma_{1\to 2} = \sigma_{1\leftrightarrow 2}$.

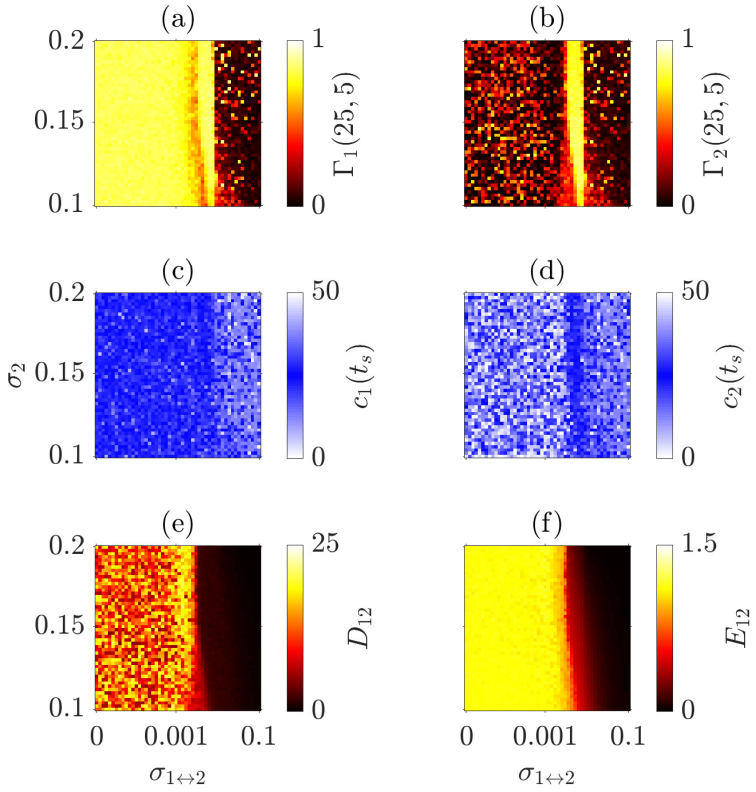

Figure 5.5: Bidirectional coupling reduces the region in which remote control is possible. Same as Figure 5.4, but here a pacemaker is present in layer 1, position $p_1 = 25$.

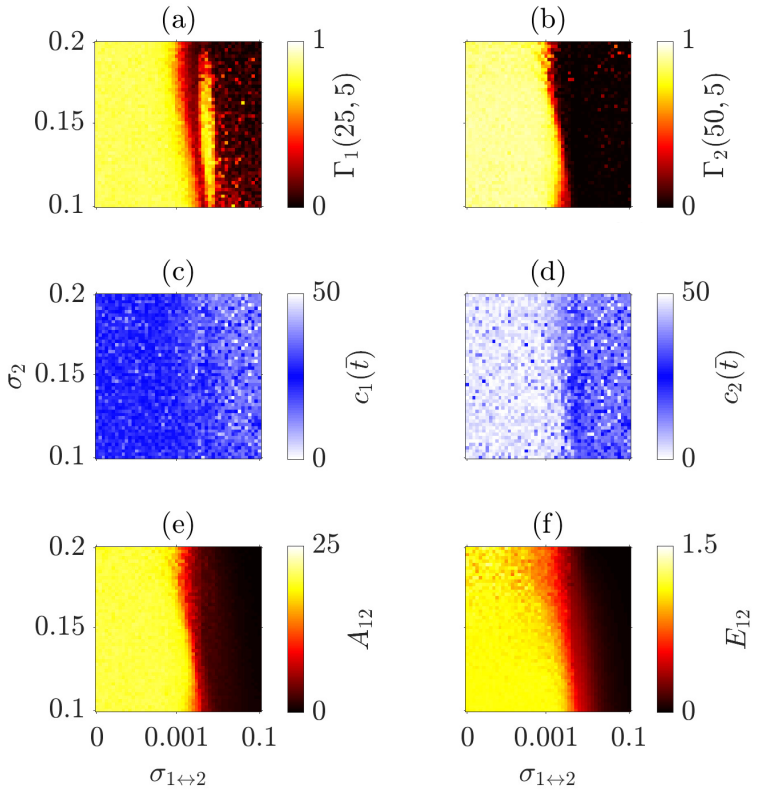

Figure 5.6: Pacemakers in different positions control chimeras in both layers and find compromise for stronger coupling. Same as Figure 5.4, but here in each layer there is a pacemaker, in position $p_1 = 25$ and $p_2 = 50$.

region of the parameter space (yellow stripe in Figure 5.5(b)).

In the third and last configuration we have conflicting pacemakers trying to control the chimera states in the two layers, one in layer 1 in position $p_1 = 25$ and one in layer 2 in position $p_2 = 50$. In this case we see that the control works in both layers in a certain region of the parameter space, corresponding to the yellow areas in Figure 5.6(a) and (b). Note that there is another small region for which the control in layer 1 continues to work. A similar effect, even more pronounced, is observed with a single pacemaker in layer 1 (Figure 5.5(a)) and is correlated with antipodal alignment in Figure 5.5(e). An analogous effect can also be observed in the transition to remote control with unidirectional coupling and a pacemaker in layer 1 (Figure 5.2(e)). For stronger interlayer coupling, the control effect ceases to exist, but the chimeras become aligned, as it is to be expected (see Figure 5.6(e)). Interestingly, the two centers are aligned but their positions do not coincide with neither of the pacemakers' positions, as we can deduce from the low values of both coupling impact measures $\Gamma_1(25, 5)$ and $\Gamma_2(50, 5)$ (rightmost part of panels (a),(b) in Figure 5.6). Looking at the center snapshots in Figure 5.6(c),(d), we see that the center is positioned close to 12.5 or 37.5 which are halfway from the pacemakers' positions. It is worth noticing that the synchronization region in Figure 5.6(f) becomes smaller when two or more pacemakers are present in the network.

5.4 Discussion

To summarize, in a two-layer multiplex network with a driver-response configuration given by unidirectional coupling between the layers, we observe a nontrivial interplay between pacemaker control of chimera states and interlayer synchronization that can be used to construct networks in which chimera states are present in

both layers and in certain positions. Furthermore, the possibility of controlling remotely the chimera states in layer 2 via a pacemaker in layer 1 is important for scenarios in which there is limited access to some parts of the network. A bidirectional coupling scheme makes the remote control of layer 2 via a pacemaker in layer 1 more difficult. When there are two conflicting pacemakers, for low values of interlayer coupling, both pacemakers attract the incoherent groups to their respective positions. As the coupling becomes stronger, the incoherent groups of the chimeras in the two layers align in a position that is halfway between the two pacemakers.

In general, we find that it is a nontrivial problem to transfer control methods for chimera states from single-layers networks to multilayer networks, given the many possible configurations in which this can be done. We show that there are ample regions of the parameter space in which the control mechanism introduced in Chapter 3 allows to control chimeras in one or both layers. The present study generalizes the finding of [82] in two directions: we go from phase to FitzHugh-Nagumo oscillators and from single-layer to multiplex networks. It will be interesting in the future to further investigate the counterintuitive effect in Figure 5.2. There the control becomes effective through a nonmonotonic process. We observe a resistance of layer 2 to being remotely controlled by layer 1, in the sense that the center of incoherence in layer 2 positions itself as far as possible from the pacemaker position before the control becomes effective.

In this chapter we saw many effects that are similar to the ones obtained for phase oscillators described in Chapter 4. There are some differences though. The most evident is that remote control with bidirectional coupling and a pacemaker in layer 1: for phase oscillators, once the control becomes effective in layer 2, it stays effective (Figure 4.6(b)), while for FitzHugh-Nagumo oscillators

the control is effective only for a limited region inside the parameter space (Figure 5.5(b)). In the case of unidirectional coupling and a pacemaker in layer 1, for phase oscillators (Figure 4.3) we did not observe the nonmonotonic behaviour that we saw for FitzHugh-Nagumo oscillators.

CHAPTER 6

Conclusion

The main contribution of this thesis is a new method to control chimera states, one of the most studied partially synchronized dynamics. This control mechanism is based on a simple idea, that of inserting a pacemaker oscillator in the network, but it provokes powerful effects. We saw how a pacemaker oscillator can induce chimera states in single-layer networks of phase oscillators and how it can also control the position of the incoherent group in this setting (Chapter 3). We also showed how even minimal modifications of the network connectivity allow one to control chimera states, and this fact indicates how the key aspect in control of chimeras is to break the spatial symmetry of the network. Moreover, we showed that the pacemaker mechanism can be used in different settings. In Chapter 4 we used the interplay of a pacemaker oscillator and the coupling betweeen two networks to control chimera states in multiplex networks of phase oscillators. In Chapter 5 we demonstrated that our control mechanism does not only work for phase oscil-

lators, but also for more complex FitzHugh-Nagumo oscillators. We also showed for which combinations of parameters the pacemaker control works in multiplex networks of FitzHugh-Nagumo oscillators. Transferring the ability of the pacemaker method to control chimera states to more realistic multilayer networks helps to bridge the gap between theoretical studies on chimera states and real-world applications.

This thesis provides several ideas for future studies. For example, for single-layer network for phase oscillators we studied how it is possible to induce a chimera state from full synchronization. It remains to be determined if this effect carries on to more complex dynamics and network topologies. The combinations of a pacemaker and multiplexing that we used in Chapter 4 and 5 are just some exemplary cases, and there are many more that can be considered. For instance, one could think about the possibility of introducing a barrier of pacemakers, and see if it can overcome the driving effect of unidirectional coupling. Moreover, in Chapter 4 we introduced a mismacth between the layer of phase oscillators via the phase-lag parameters and in Chapter 5 via the intralayer coupling for FitzHugh-Nagumo oscillators. Of course there are many other possible parameters to choose from to further test the robustness of our results. Finally, the most interesting future development of the present study would probably be to see the method introduced here in some experimental setting, to help sustaining these partially synchronized states.

Bibliography

[1] H. D. I. Abarbanel, N. F. Rulkov, and M. M. Sushchik. Generalized synchronization of chaos: The auxiliary system approach, *Physical Review E* 53 (1996), 4528.

[2] D. Abrams et al. Solvable model for chimera states of coupled oscillators, *Physical Review Letters* 101 (2008), 084103.

[3] D. M. Abrams and S. H. Strogatz. Chimera states for coupled oscillators, *Physical Review Letters* 93 (2004), 174102.

[4] A. Aleta and Y. Moreno. Multilayer networks in a nutshell, *Annual Reviews of condensed matter physics* 10 (2019), 45–62.

[5] R. G. Andrzejak, G. Ruzzene, and I. Malvestio. Generalized synchronization between chimera states, *Chaos: an interdisciplinary journal of nonlinear science* 27 (2017), 053114.

[6] R. G. Andrzejak et al. All together now: Analogies between chimera state collapses and epileptic seizures, *Scientific Reports* 6 (2016), 23000.

[7] R. G. Andrzejak et al. Mean field phase synchronization between chimera states, *Chaos: an interdisciplinary journal of nonlinear science* 28 (2018), 091101.

[8] R. G. Andrzejak et al. Two populations of coupled quadratic maps exhibit a plentitude of symmetric and symmetry broken dynamics, *Chaos: an interdisciplinary journal of nonlinear science* 30 (2020), 033125.

[9] T. Banerjee et al. Chimera patterns induced by distance-dependent power-law coupling in ecological networks, *Physical Review E* 94 (2016), 032206.

[10] K. Bansal et al. Cognitive chimera states in human brain networks, *Science Advances* 5 (2019), 8536.

[11] V. M. Bastidas et al. Quantum signatures of chimera states, *Physical Review E* 92 (2015), 062924.

[12] F. Battiston et al. Multilayer motif analysis of brain networks, *Chaos: an interdisciplinary journal of nonlinear science* 27 (2017), 047404.

[13] C. Bick and E. A. Martens. Controlling chimeras, *New Journal of Physics* 17 (2015), 33030.

[14] C. Bick, M. Sebek, and I. Z. Kiss. Robust weak chimeras in oscillator networks with delayed linear and quadratic interactions, *Physical Review Letters* 119 (2017), 168301.

[15] S. Boccaletti et al. *Synchronization: From coupled systems to complex networks*. Cambridge University Press, 2018.

[16] S. Boccaletti et al. The structure and dynamics of multilayer networks, *Physics Reports* 544 (2014), 1–122.

[17] S. Bogomolov et al. Amplitude and phase chimeras in an ensemble of chaotic oscillators, *Technical Physics Letters* 42 (2016), 765–768.

[18] S. A. Bogomolov et al. Mechanisms of appearance of amplitude and phase chimera states in ensembles of nonlocally coupled chaotic system, *Communicationts in Nonlinear Science and Numerical Simulations* 43 (2017), 25–36.

[19] A. zur Bonsen et al. Chimera states in networks of logistic maps with hierarchical connectivities, *European Physical Journal B* 91 (2018), 65.

[20] A. Bukh et al. New type of chimera and mutual synchronization of spatiotemporal structures in two coupled ensembles of nonlocally interacting chaotic maps, *Chaos: an interdisciplinary journal of nonlinear science* 27 (2017), 111102.

[21] P. Chandran et al. Chimera states in coupled logistic maps with additional weak nonlocal topology, *Chaos: an interdisciplinary journal of nonlinear science* 29 (2019), 053125.

[22] T. Chouzouris et al. Chimera states in brain networks: Empirical neural vs. modular fractal connectivity, *Chaos: an interdisciplinary journal of nonlinear science* 28 (2018), 045112.

[23] R. FitzHugh. Impulses and physiological states in theorethical models of nerve membrane, *Biophysics Journal* 1 (1961), 445.

[24] R. Gallotti and M. Berthelemy. The multilayer temporal network of public transport in Great Britain, *Scientific Data* 2 (2015), 140056.

[25] L. V. Gambuzza and M. Frasca. Pinning control of chimera states, *Physical Review E* 94 (2016), 022306.

[26] L. V. Gambuzza et al. Experimental investigation of chimera states with quiescent and synchronous domains in coupled electronic oscillators, *Physical Review E* 90 (2014), 032905.

[27] S. Ghosh, A. Zakharova, and S. Jalan. Non-identical multiplexing promotes chimera states, *Chaos, Solitons and Fractals* 106 (2018), 56–60.

[28] S. Ghosh et al. Birth and death of chimeras: Interplay of delay and multiplexing, *Europhysics Letters* 115 (2016), 60005.

[29] S. Ghosh et al. Taming chimeras in networks through multiplexing delays, *Europhysics Letters* 127 (2019), 30002.

[30] A. Gjurchinovski, E. Schöll, and A. Zakharova. Control of amplitude chimeras by time delay in oscillator networks, *Physical Review E* 95 (2017), 042218.

[31] J. C. González-Avella, M. G. Cosenza, and M. San Miguel. Localized coherence in two interacting populations of social agents, *Physica A: Statistical Mechanics and its Applications* 399 (2014), 24–30.

[32] M. V. Goremyko et al. Interaction of chimera states in a multilayereed network of nonlocally coupled oscillators, *Technical Physics Letters* 43 (2017), 712–715.

[33] A. M. Hagerstrom et al. Experimental observation of chimeras in coupled-map lattices, *Nature Physics* 8 (2012), 658–661.

[34] J. D. Hart et al. Experimental observation of chimera and cluster states in a minimal globally coupled network, *Chaos: an interdisciplinary journal of nonlinear science* 26 (2016), 094801.

[35] J. D. Hart et al. Experiments with arbitrary networks in time-multiplexed delay systems, *Chaos: an interdisciplinary journal of nonlinear science* 27 (2017), 111102.

[36] J. Hizanidis et al. Chimera states in networks of nonlocally coupled Hindmarsh-Rose neuron models, *International Journal of Bifurcation and Chaos* 24 (2014), 1450030.

[37] A. L. Hodgkin and A. F. Huxley. A quantitative description of membrane current and its applications to conduction and excitation in nerve, *The Journal of Physiology* 117 (1952), 500–544.

[38] T. Isele et al. Controlling chimera states: The influence of excitable units, *Physical Review E* 93 (2016), 022217.

[39] P. Kalle et al. Chimera states and the interplay between initial conditions and non-local coupling, *Chaos: an interdisciplinary journal of nonlinear science* 27 (2017), 033110.

[40] L. Kang et al. A two-layered brain network model and its chimera state, *Scientific Reports* 9 (2019), 14389.

[41] T. Kasimatis, J. Hizanidis, and A. Provata. Three-dimensional chimera patterns in networks of spiking neuron oscillators, *Physical Review E* 97 (2018), 052213.

[42] M. Kivelä et al. Multilayer networks, *Journal of Complex Networks* 2 (2014), 203–271.

[43] H. Kori and A. S. Mikhailov. Entrainment of Randomly Coupled Oscillator Networks by a Pacemaker, *Physical Review Letters* 93 (2004), 254101.

[44] N. E. Kouvaris et al. Chimera states in a network-organized public goods game with destructive agents, *Chaos: an interdisciplinary journal of nonlinear science* 26 (2016), 123108.

[45] S. Kundu, S. Majhi, and D. Ghosh. From asynchronous to synchronous chimeras in ecological multiplex networks, *The European Physical Journal Special Topics* 228 (2019), 2429–2439.

[46] Y. Kuramoto. Self-entrainment of a population of coupled non-linear oscillators, *International Symposium on Mathematical Problems in Theoretical Physics* 39 (1975).

[47] Y. Kuramoto and D. Battogtokh. Coexistence of Coherence and Incoherence in Nonlocally Coupled Phase Oscillators, *Nonlinear Phenomena in Complex Systems* 4 (2002), 380–385.

[48] C. R. Laing. Dynamics and stability of chimera states in two coupled populations of oscillators, *Physical Review E* 100 (2019), 042211.

[49] L. Larger, B. Penkovsky, and Y. Maistrenko. Virtual Chimera States for Delayed-Feedback Systems, *Physical Review Letters* 111 (2013), 054103.

[50] J. Lenhert. *Controlling synchronization patterns in complex networks*. Springer, 2015.

[51] S. A. M. Loos et al. Chimera patterns under the impact of noise, *Physical Review E* 93 (2016), 012209.

[52] Y. Maistrenko, B. Penkovsky, and M. Rosenblum. Solitary states at the edge of synchrony in ensembles with attractive and repulsive interactions, *Physical Review E* 89 (2014), 060901.

[53] Y. Maistrenko et al. Chimera states in three dimensions, *New Journal of Physics* 17 (2015), 073037.

[54] S. Majhi, M. Perc, and D. Ghosh. Chimera states in a multilayer network of coupled and uncoupled neurons, *Chaos: an interdisciplinary journal of nonlinear science* 27 (2017), 073109.

[55] S. Majhi, M. Perc, and D. Ghosh. Chimera states in uncoupled neurons induced by a multilayer structure, *Scientific Reports* 6 (2016), 39033.

[56] S. Majhi et al. Chimera states in neuronal networks: a review, *Physics of Life Reviews* 28 (2018), 100–121.

[57] V. A. Maksimenko et al. Excitation and suppression of chimera states by multiplexing, *Physical Review E* 94 (2016), 052205.

[58] E. A. Martens et al. Chimera states in mechanical oscillator networks, *Proceedings of the National Academy of Sciences* 110 (2013), 10563–10567.

[59] M. Mikhaylenko et al. Weak multiplexing in neural networks: Switching between chimera and solitary states, *Chaos: an interdisciplinary journal of nonlinear science* 29 (2019), 023122.

[60] E. Montbrió, J. Kurths, and B. Blasius. Synchronization of two interacting populations of oscillators, *Physical Review E* 70 (2008), 056125.

[61] J. Nagumo, S. Arimoto, and S. Yoshizawa. An active pulse transmission line simulating nerve axon, *Proceedings of the IRE* 50 (1962), 2061–2070.

[62] C. R. Nayak and N. Gupte. Chimera states in coupled sine-circle map lattices, *AIP Conference Proceedings* 1339 (2011), 172–180.

[63] I. Omelchenko et al. Control of chimera states in multilayer networks, *Frontiers in Applied Mathematics and Statistics* 4 (2019), 67.

[64] I. Omelchenko et al. Loss of coherence in dynamical networks: Spatial chaos and chimera states, *Physical Review Letters* 106 (2011), 234102.

[65] I. Omelchenko et al. Nonlinearity of local dynamics promotes multi-chimeras, *Chaos: an interdisciplinary journal of nonlinear science* 25 (2015), 083104.

[66] I. Omelchenko et al. Optimal design of tweezer control for chimera states, *Physical Review E* 97 (2018), 012216.

[67] I. Omelchenko et al. Tansition from spatial coherence to incoherence in coupled chaotic systems, *Physical Review E* 85 (2012), 026212.

[68] I. Omelchenko et al. Tweezers for Chimeras in Small Networks, *Physical Review Letters* 116 (2016), 114101.

[69] I. Omelchenko et al. When nonlocal coupling between oscillators becomes stronger: Patched synchrony or multichimera states, *Physical Review Letters* 110 (2013), 224101.

[70] O. E. Omel'chenko. The mathematics behind chimera states, *Nonlinearity* 31 (2018), R121.

[71] O. E. Omel'chenko and E. Knobloch. Chimerapedia: coherence-incoherence patterns in one, two and three dimensions, *New Journal of Physics* 21 (2019), 093034.

[72] O. E. Omel'chenko, M. Wolfrum, and Y. L. Maistrenko. Chimera states as chaotic spatiotemporal patterns, *Physical Review E* 81 (2010), 065201.

[73] M. J. Panaggio et al. Chimera states in networks of phase oscillators: The case of two small populations, *Physical Review E* 93 (2016), 012218.

[74] A. Pikovsky, M. Rosenblum, and J. Kurths. *Synchronization - A universal concept in nonlinear sciences*. Cambridge University Press, 2001.

[75] A. Pournaki et al. Synchronization patterns in modular neuronal networks: a case study of C. elegans, *Frontiers in Applied Mathematics and Statistics* 5 (2019), 52.

[76] A. Provata and G. Argyropolous. Chimera states with 2D deterministic and random fractal connectivities, *Frontiers in applied mathematics and statistics* 5 (2019), 35.

[77] F. Radicchi and H. Meyer-Ortmanns. Entrainment of coupled oscillators on regular networks by pacemakers, *Physical Review E* 73 (2006), 036218.

[78] L. Ramlow et al. Partial synchronization in empirical brain networks as a model for uniemispheric sleep, *EuroPhysics Letters* 126 (2019), 50007.

[79] N. C. Rattenborg, C. J. Amlaner, and S. L. Lima. Behavioral, neurophysiological and evolutionary perspectives on uniemispheric sleep, *Neuroscience and biobehavioral reviews* 24 (2000), 817.

[80] M. G. Rosenblum, A. S. Pikovsky, and J. Kurths. Phase synchronization of chaotic oscillators, *Physical Review Letters* 76 (1995), 1804–1907.

[81] N. F. Rulkov et al. Generalized synchronization of chaos in directionally coupled chaotic systems, *Physical Review E* 51 (1995), 980–994.

[82] G. Ruzzene et al. Controlling chimera states via minimal coupling modification, *Chaos: an interdisciplinary journal of nonlinear science* 29 (2019), 051103.

[83] G. Ruzzene et al. Remote pacemaker-control of chimera states in multilayer networks of neurons, *in preparation* (2020).

[84] E. Rybalova et al. Spiral and target-wave chimeras in a 2D lattice of map-based neuron models, *Chaos: an interdisciplinary journal of nonlinear science* 29 (2019), 101104.

[85] E. V. Rybalova, G. Strelkova, and V. Anischenko. Mechanism of realizing a solitary state chimera in a ring of nonlocally coupled chaotic maps, *Chaos Solitons Fractals* 115 (2018), 300.

[86] E. V. Rybalova et al. Forced synchronization of a multilayer heterogeneous network of chaotic maps in the chimera state mode, *Chaos: an interdisciplinary journal of nonlinear science* 29 (2019), 033134.

[87] J. Sawicki et al. Delay controls chimera relay synchronization in multiplex networks, *Physical Review E* 98 (2018), 062224.

[88] J. Sawicki et al. Delay-induced chimeras in neural networks with fractal topology, *The European Physical Journal B* 92 (2019), 54.

[89] J. Sawicki et al. Synchronization scenarios of chimeras in multiplex networks, *The European Physical Journal Special Topics* 270 (2018), 1161–1171.

[90] L. Schmidt et al. Coexistence of synchrony and incoherence in oscillatory media under nonlinear global coupling, *Chaos: an interdisciplinary joournal of nonlinear science* 24 (2014), 013102.

[91] L. Schülen et al. Delay engineered solitary states in complex networks, *Chaos, Solitons and Fractals* 128 (2019), 290–296.

[92] N. Semenova et al. Does hyperbolicity impede the emergence of chimera states in networks of nonlocally coupled chaotic oscillators?, *Europhysics Letters* 112 (2015), 40002.

[93] N. Semenova et al. Temporal intermittency and the lifetime of chimera states in ensembles of nonlocally coupled chaotic oscillators, *Chaos: an Interdisciplinary journal of nonlinear science* 27 (2017), 061102.

[94] J. H. Sheeba, V. K. Chandrasekar, and M. Lakshmanan. Globally clustered chimera states in delay-coupled populations, *Physical Review E* 79 (2009), 055203.

[95] I. A. Shepelev et al. Chimera states in ensembles of bistable elements with regular and chaotic dynamics, *Nonlinear Dynamics* 90 (2017), 2317–2330.

[96] J. Sieber, O. E. Omel'chenko, and M. Wolfrum. Controlling unstable chaos: Stabilizing chimera states by feedback, *Physical Review Letters* 112 (2014), 054102.

[97] G. I. Strelkova, T. E. Vadivasova, and V. S. Anischenko. Synchronization of chimera states in a network of many unidirectionally coupled layers of discrete maps, *Regular and chaotic Dynamics* 23 (2018), 948–960.

[98] Y. Suda and K. Okuda. Persistent chimera states in nonlocally coupled phase oscillators, *Physical Review E* 92 (2015), 060901.

[99] M. R. Tinsley, S. Nkomo, and K. Showalter. Chimera and phase-cluster states in populations of coupled chemical oscillators, *Nature Physics* 8 (2012), 662–665.

[100] J. F. Totz et al. Spiral wave chimera states in large populations of coupled chemical oscillators, *Nature Physics* 14 (2018), 282–285.

[101] G. I. Vadisova T. E. Strelkova, S. A. Bogomolov, and V. S. Anischenko. Correlation analysis of the coherence-incoherence transition in a ring of nonlocally coupled logistic maps, *Chaos: an interdisciplinary journal of nonlinear science* 26 (2016), 093108.

[102] M. Wickramasinghe and I. Z. Kiss. Spatially organized dynamical states in chemical oscillator networks: Synchronization, dynamical dierentiation, and chimera patterns, *PLoS ONE* 8 (2013), e80586.

[103] A. T. Winfree. Biological rhythms and the beahoviour of coupled oscillators, *Journal of theorethical biology* 16 (1967), 15–42.

[104] M. Winkler et al. Relay synchronization in multiplex networks of discrete maps, *Europhysics Letters* 126 (2019), 50004.

[105] M. Wolfrum and O. E. Omel'chenko. Chimera states are chaotic transients, *Physical Review E* 84 (2011), 015201.

[106] N. Yao et al. Self-adaptation of chimera states, *Physical Review E* 99 (2019), 010201.

[107] A. Zakharova. *Chimera patterns in networks: Interplay between dynamics, structure, noise and delay*. Springer, 2019.

[108] A. Zakharova, M. Kapeller, and E. Schöll. Amplitude chimeras and chimera death in dynamical networks, *Journal of Physics: Conference Series* 727 (2016), 010218.